This manuscript is a pre-print version that has been submitted for peer-review to Basin Research. Content of this manuscript may be updated in future versions.

Structural Evolution of Salt-Influenced Fold-and-Thrust Belts: Principles in Salt Basins Containing Isolated Minibasins

Oliver B. Duffy[1], Tim P. Dooley[1], Michael R. Hudec[1], Naiara Fernandez[1], Christopher A-L. Jackson[2], Juan I. Soto[1*]

[1]Bureau of Economic Geology, Jackson School of Geosciences, The University of Texas at Austin, University Station, Box X, Austin, Texas, 78713-8924, USA

[2]Basins Research Group (BRG), Department of Earth Science & Engineering, Imperial College, Prince Consort Road, London, United Kingdom, SW7 2BP

[*]On leave of absence from: Departamento de Geodinámica and Instituto Andaluz de Ciencias de la Tierra (CSIC-UGR), Universidad de Granada, Avenida de Fuente Nueva s/n, 18071 Granada, Spain

Corresponding author: Oliver Duffy (oliver.duffy@beg.utexas.edu)

Highlights:

- In settings with isolated minibasins and a high salt volume, shortening induces salt flow
- The flow of salt contributes to the translation, tilt and rotation of minibasins during shortening
- A variety of factors control the amount and timing of minibasin translation, tilt and rotation during shortening
- The controls include, amongst others: boundary conditions, salt pressures, base-salt relief, whether primary and secondary welds have formed
- Fold-and-thrust belts in salt basins can vary in style, being strongly influenced by the volume and distribution of precursor salt

Abstract

Shortening styles in salt-influenced fold-and-thrust belts can vary markedly, with the volume and distribution of salt prior to shortening being a key control. Here we use a suite of physical models to examine styles of thin-skinned shortening in settings where the precursor structure comprised minibasins surrounded by salt (‘isolated-minibasin’ provinces). Our models show that the high volume of mechanically-weak salt localizes shortening and induces salt flow, and that this salt flow contributes to three key processes - translation, tilting and rotation of minibasins. First, we demonstrate that salt flowing around minibasins propels them in the shortening direction, with translation enhanced by fast-flowing salt streams and impeded by basal friction and buttresses. Second, we show how minibasin tilt directions and magnitudes vary spatially and temporally during shortening. Minibasins tilt away from zones of pressurized salt, the locations of which may shift due to changes in salt flow. Tilts may also change as minibasins pivot on primary welds, or due to forces associated with minibasin collision. Third, minibasins can rotate around steep axes during shortening. We speculate that this rotation is caused by a combination of: i) tractions imparted on the minibasin boundary by flow of adjacent salt; and ii) pivoting on welds. We synthesize our results in a series of 3-D conceptual models. Finally, we compare and contrast shortening styles and processes in salt-influenced fold-and-thrust belts with different pre-shortening salt configurations.

1 Salt-Influenced Fold-and-Thrust Belts: Thin-Skinned Styles

Salt-influenced fold-and-thrust-belts are common in orogenic settings and in the down-dip contractional domains of salt-detached slope systems, displaying a wide range of structural styles (e.g. Davis and Engelder, 1985; Letouzey et al., 1995; Rowan and Vendeville, 2006; Callot et al., 2007; Morley et al., 2011; Lacombe and Bellahasen, 2016; Duffy et al., 2018; Granado et al., 2018; Dooley et al., 2019; Legeay et al., 2019). This diversity in structural style arises during shortening due to: i) the strength difference between the relatively weak salt and relatively strong sedimentary rocks; ii) variations in the number of salt detachment levels, and iii) the heterogeneous distribution of salt prior to shortening, a function of salt's mobility, and in some areas the irregular deposition of salt across rugose topography. In particular, previous studies have shown how the proportion and distribution of mechanically weak salt in a system will significantly impact the structural styles that develop as it shortens (Davis and Engelder, 1985; Letouzey et al., 1995; Cotton and Koyi, 2000; Rowan and Vendeville, 2006; Callot et al., 2007; Dooley et al., 2009; Darnault et al., 2016; Duffy et al., 2017; 2018; Jackson and Hudec, 2017; Butler, 2019; Legeay et al., 2019). Three end-member configurations of salt typically exist prior to shortening: i) an undeformed flat- or gently-dipping salt layer; ii) an array of isolated stocks or walls encased in a relatively rigid sediment body ('isolated diapirs'; Figure 1a); and iii) the focus of this study, settings where minibasins are surrounded by salt ('isolated minibasins', Duffy et al., 2018 and Dooley et al., 2019; Fig. 1b). Shortened isolated-minibasin settings have previously been termed Wall-and-Basin settings (WAB), and can include systems with multiple generations of minibasins and salt canopies (e.g. Harrison and Jackson., 2014; Flinch and Soto, 2017; Kergaravat et al., 2017). In this study we focus on styles of thin-skinned ('supra-salt') shortening, though we recognize that many salt-influenced fold-and-thrust belts may have additional thick-skinned components (e.g. Legeay et al., 2019).

Where bedded salt is initially undeformed, a basal detachment can form within it during shortening, with a fold-and-thrust belt developing within its overburden (e.g. Davis and Engelder, 1985; Letouzey et al., 1995; Costa and Vendeville, 2002; Morley et al., 2011). Such thin-skinned fold-and-thrust belts are typically characterized by: i) an extremely low cross-sectional taper, with folds and thrusts developed across a wide belt; ii) abrupt changes in structural style at the edges of the salt basin where deformation is concentrated; iii) regularly-spaced salt-bearing thrusts, broad, box-like synclines, and narrow, symmetric, salt-cored anticlines; and iv) a remarkable continuity of structural style, which may extend 10's or 100s of kilometers along-strike (e.g. Davis and Engelder, 1985; Letouzey et al., 1995; Morley et al., 2011) (Fig. 2). Natural examples of such settings include the Valley and Ridge Province of the Appalachians, USA (e.g. Frey, 1973), the Alps and the Jura Mountains, Switzerland and France (e.g. Laubscher, 1961; Guellec et al., 1990; Sommaruga et al., 2017; Leitner and Spötl, 2017), the Salt Range, Pakistan (e.g. Grelaud et al., 2002), the Sub-Andean foreland in Peru and Bolivia (e.g. Hermoza et al., 2005; Baby et al. 2018; McClay et al., 2018), and the Northwestern Zagros Mountains, Iran (e.g. Sherkati et al., 2006; Dooley et al., 2007) (see Davis and Engelder, 1985 for a more complete list).

Where diapirs have formed prior to shortening, they preferentially localize shortening strain such that they narrow and rise as they are squeezed. In contrast, at low strains, the comparatively strong surrounding sedimentary rocks remain mostly undeformed (e.g. Nilsen et al., 1995; Rowan and Vendeville, 2006; Callot et al., 2007; Dooley et al., 2009; 2013; Duffy et al., 2018; Legeay et al., 2019). Duffy et al (2018) synthesize how isolated-diapir provinces shorten using observations from published natural examples such as the Fars Region of the Zagros

Mountains, Iran (e.g. Callot et al., 2007; 2012) and the Astrid Fold Belt (e.g. Jackson et al., 2008) in the Lower Congo Basin, Gabon, as well as data from published and new physical models (e.g. Callot et al., 2007; Dooley et al., 2009a; 2009b; 2015). They show that in shortened isolated-diapir systems, faults and folds typically nucleate at diapirs before propagating out into flanking sedimentary rocks (e.g. Snidero et al., 2019). These structures connect with those from adjacent diapirs to form a network, with the style and orientation of the structures largely determined by the pre-shortening configuration of diapirs within the array (e.g. Callot et al., 2007; Dooley et al., 2009; Duffy et al., 2018). Duffy et al. (2018) surmise that the relatively low volume of salt, and the isolated and poorly-connected nature of the salt bodies in isolated-diapir settings, results in a thin-skinned system that behaves in a mechanically relatively rigid manner during shortening. Critically, shortened isolated-diapir settings show greater spatial variability in structural style than fold-and-thrust belts developed above an initially undeformed salt decollement.

In contrast to shortened isolated-diapir settings, a detailed understanding of the processes and controls on thin-skinned shortening in isolated-minibasin settings remains largely unknown. Prior to shortening, settings such as the southeast portion of the Precaspian Basin, Kazakhstan (e.g. Duffy et al., 2017; Fernandez et al., 2017; Jackson et al., 2019) and the central portion of the Sivas Basin (central domain), Turkey (Ringenbach et al., 2013; Callot et al., 2014; Kergaravat et al., 2016; 2017; Ribes et al., 2017; Legeay et al., 2019), are interpreted to have had a high salt volume (Fig. 1b) with each minibasin surrounded by a polygonal network of connected salt walls in map-view. Isolated-minibasin systems are less mechanically-rigid during shortening than isolated-diapir settings, given the minibasins are prone to be essentially disconnected from one another and mobile. As such the minibasins have the potential to behave independently, with significant implications for resulting structural styles (e.g. Rowan and Vendeville, 2006; Legeay et al., 2019).

Fundamental questions remain about how and why the mobile and isolated minibasins translate, tilt (i.e. around a horizontal axis) and rotate (i.e. around a vertical axis) during shortening.

To address these questions, we first review the fundamental mechanical principles that control structural styles developed in shortened isolated-minibasin provinces. We couple this review with observations from a suite of new physical models designed to explore key processes that occur as isolated minibasin provinces shorten – minibasin translation, tilting, and rotation. We then synthesise our findings in a series of 3D conceptual models. Finally, we assess the wider implications of our work, by comparing and contrasting shortening styles and processes in salt-influenced fold-and-thrust belts with different pre-shortening configurations. Our findings contribute to the growing body of literature highlighting how the geometry and kinematics of fold-and-thrust belts worldwide are strongly controlled by the initial volume and distribution of salt.

2 Governing Principles and Characteristics of Shortened Isolated-Minibasin Provinces

The general principles of isolated-minibasin shortening are outlined by Rowan and Vendeville (2006). Using physical models, they show that shortening is preferentially accommodated by the weak salt surrounding the minibasins. In particular, precursor salt walls oriented perpendicular to the shortening direction narrow or weld shut during shortening. In contrast, diapirs oriented parallel to the shortening direction widen and forms strike-slip shear zones, whereas those oriented oblique to the shortening direction typically host oblique-slip transpressional shear zones (Rowan and Vendeville, 2006) (Fig. 3). Importantly, as the salt deforms during shortening, the strong minibasins are mobile and translate independently of one another. Thus, minibasins may converge, diverge, and collide, as well as rotate around horizontal, and vertical axes (Rowan and Vendeville, 2006).

With these concepts in mind, it is possible to observe a fold-and-thrust belt and look for first-order diagnostic features that would indicate if it derived from shortening of an isolated-minibasin province. In map-view, diagnostic features include the presence of closely-spaced or welded, ovate minibasins. These minibasins may be bounded either by a polygonal to irregular network of salt walls or an equivalent pattern of welds. Salt walls trending in one orientation tend to be narrower or preferentially welded-out, whereas those trending orthogonal tend to be wider (Fig. 3). Furthermore, the map-view distribution of extensional, contractional, and strike-slip deformation at the minibasin boundaries should be complex due to jostling between the mobile minibasins as they were packed close together (Fig. 3) (Rowan and Vendeville, 2006; Granado et al. 2018; Legeay et al., 2019). In section-view, diagnostic features can include the presence of internally-undeformed minibasins, extreme minibasin tilts, and highly spatially-variable structural styles (Rowan and Vendeville, 2006; Kergaravat et al., 2016, 2017; Ribes et al. 2017; Duffy et al., 2017; Legeay et al., 2019). Critically, structural restorations, salt volume estimates, and the tectono-stratigraphic history of the setting must be compatible with the principle of isolated minibasins having been initiated prior to shortening (e.g. salt volumes must be relatively high).

Shortened isolated-minibasin provinces occur in the Southeast Precaspian Basin, Kazakhstan (e.g. Duffy et al., 2017; Fernandez et al., 2017; Jackson et al., 2019), the central portion of the Sivas Basin, Turkey (Ringenbach et al., 2013; Callot et al., 2014; Kergaravat et al., 2016; 2017; Legeay et al., 2019), Axel-Heiberg Island, Arctic Canada (e.g. Harrison and Jackson, 2014), the Northern Calcareous Alps, Austria (Granado et al., 2018), the Betics, southern Spain (Flinch and Soto, 2017), the Flinders Range, South Australia (Rowan and Vendeville, 2006), and portions of contractional domains on the salt-detached slope above the Sigsbee canopy in the Northern Gulf of Mexico (Duffy et al. 2019; Fernandez et al. 2020) (e.g. Fig. 4).

However, fundamental questions remain regarding the thin-skinned processes that occur as isolated-minibasin provinces shorten. These questions include: 1) Why do minibasins translate and what factors may enhance or inhibit translation? 2) What factors influence the variable tilts we see in natural shortened isolated-minibasin provinces? (*cf*. Fig. 4c and d); and 3) do minibasins rotate around vertical (or steep) axes, and if so, what factors influence this? To address these questions, we will present key observations from a suite of new physical models, highlighting the importance of salt flow, minibasin interaction, and base-salt relief.

.

3 Physical-Modelling Approach

In this paper we use the results of three physical models involving a variety of arrays of isolated minibasins sinking into a "sea" of salt to investigate processes such as minibasin mobility, minibasin tilting and minibasin rotation during shortening (Figure 5; see details below). As with other physical modeling studies of salt tectonics, we simulated rock salt using ductile silicone and its siliciclastic overburden using brittle, dry, granular material. The silicone was a near-Newtonian viscous polydimethylsiloxane. This polymer has a density of 950 to 980 kg m^{-3} and a dynamic shear viscosity of 2.5×10^4 Pa s at a strain rate of 3×10^{-1} s^{-1} (Weijermars, 1986; Weijermars et al., 1993). In some of our models the salt analog was dyed with minute quantities of powdered pigments in order to track salt flow paths in the completed model (see Dooley et al., 2009, for further details). Our granular minibasin infills comprised different colored mixtures of silica sand (bulk density of ~1,700 kg m^{-3}; grain size of 300-600 μm; internal friction coefficient, μ, = 0.55–0.65; McClay, 1990; Krantz, 1991; Schellart, 2000), and hollow ceramic microspheres (“glass beads”) having a bulk density of 650 kg m^{-3}, average grain size 90-150 μm, and typical μ = 0.45 (e.g. Rossi and Storti, 2003; Dooley et al., 2009). The hollow spheres serve to lower bulk grain size, as well as allowing us to modify the bulk density of the suprasalt section and to seed minibasins that had a density stratification. In all of our models the minibasins were initially seeded using outward-widening circular templates. Minibasins possessed a dense narrow core of our granular mixture with a density 1.4-times that of our salt analog, fringed by a wider circular template with a density 1.2-times that of our salt analog, and finally passing out into an outer fringe with a density equal to that of our salt analog. Initially our minibasins possessed positive topography but sank over several hours to produce negative topography with a bowl-shaped profile. Minibasin infill then infilled negative relief to top salt, firstly as they subsided into the salt basin and then as the salt massifs rose around the transported minibasins during shortening, recording the subsidence history as well as the tilting history of each individual minibasin. This “fill-to-top” approach inhibits encasement or canopy formation above the minibasin array.

Computer-controlled cameras photographed the obliquely-lit upper and basal surfaces of the models at set time intervals. A digital image correlation (DIC) system, consisting of a high-resolution stereo charge-coupled device system and associated software, tracked the surface-strain history, subsidence, and uplift values, as well as displacement vectors of the top, and where relevant, basal surfaces of the model. The speckled nature of the sand and cenosphere mixtures used in our models are ideal for this type of monitoring system (see Reber et al., 2020 for further details). Adding syn-kinematic layers means data is incremental for individual layers deposited during subsidence and shortening stages of our models. We use two main types of DIC maps in this paper: (1) height-change maps that pick our minibasin tilting and the rising salt massifs, and: (2) maps showing displacement in the shortening direction (eastwards) that highlight fast and slow moving parts of the system. In all cases, where we show height change or displacement maps the values are calculated over the period of the most recent minibasin infill cycle. For more details on DIC monitoring techniques the reader is referred to Adam et al. (2005). After completion models were impregnated with a gelatin mixture, left to partially dry for 12 hours and then sliced into closely spaced slabs. Coregistered digital photographs of these closely spaced serial sections (≤3.5 mm apart) yielded a 3D voxel of the completed model. Dip sections are the sliced and photographed cross sections, whereas crosslines, arbitrary lines and depth slices are virtual sections constructed from the voxel model. As a result, the crossline, arbitrary line and depth slice images are interpolated and thus not as sharp as those derived directly from photographed dip sections.

The setup of the three models used in this study are schematically illustrated in Figure 5 along with various parameters. Models 1a and b consisted of an array of minibasins subjected to shortening once they had subsided deeply into our salt basin. The goal of this model set was to test the impact of minibasin depth, and welding, on initial minibasin mobility. Primary and secondary welding also occurred in this model set and we document the impact of these processes on mobility and minibasin tilting. Note that the salt basin in Model 1 abruptly terminates east of the minibasin array and thus contractional thickening of our salt analog occurred at this side of the rig during shortening. In nature this could be the actual edge of the salt basins, where mobility abruptly halts, or it could be a less mobile part of the salt basin where minibasins have already strongly welded at base of salt.

Model 2 tested the impact of a plunging base-of-salt high block on minibasin mobility and tilting (Figure 5). And finally, Model 3 tested the impact of an array of intrasalt minibasins on salt flow and suprasalt minibasin translation, secondary welding, and rotation during shortening.

4 Minibasin Translation During Shortening

Why do minibasins translate during shortening? The fundamental process driving minibasin translation during shortening is captured in the results from the Model 1 set (setup shown in Fig. 5). As the moving endwall shortens the initial configuration, salt preferentially absorbs the shortening strain and flows eastwards towards the foreland, expelling from between the minibasins, and thickening in the absence of a mechanically-significant roof (Fig. 6) (see physical modelling movies in Dooley, 2020). Critically, this flowing salt propels the minibasins eastwards (Fig. 6). As they translate, the relatively strong minibasins do not deform internally, as shown by the consistent translation magnitudes within them (color indicating the shortening-parallel (eastwards) displacement of the top model surface is broadly consistent across each minibasin on Fig. 6). Furthermore, as we see salt thicken around the minibasins as the system shortens, it means that in natural shortened basins where the initial salt basin area is unknown, minibasin thickness cannot be used as a proxy for original salt thickness.

What controls how far and how fast a minibasin translates during shortening? At the largest scale, a major control on minibasin translation is the direction of strain propagation. Results from Model 1a show strain propagates eastwards through the system, as indicated by the greater displacement of salt near the moving endwall (Fig. 6). The eastwards decrease in salt flow magnitude means minibasins closer to the moving endwall are propelled more-strongly by flowing salt and thus translate at higher velocities (orange and green colored minibasins) than those further east (purple and blue colored minibasins) (Fig. 6). Model 1a results also suggest that the velocity of translation of every minibasin decreases as cumulative shortening increases (*cf*. change in color of each minibasin between Figs 6a and b). We explain this by the fact that sediments were continually added to the minibasins during shortening and thus they thickened during shortening. The result being that the thickness of salt beneath each of the minibasins decreased during shortening, and we summise that the thinner the salt beneath a minibasin, the lower its translation velocity (cf. 6a and 6b).

Local-scale variations in salt flow velocity can also influence how far and how fast minibasins translate during shortening. We can explore this in Model 1a in which as salt near the moving endwall flows eastward, it encounters relatively thick (likely welded) Minibasin 3 (Fig. 6a). This minibasin is not translating basinwards as fast as the salt to its west (SMB3 has lower shortening-parallel (eastwards) displacements (light-green color) than the salt (orange color)), and it thus it forms a barrier to the eastward-flowing salt. Eastward-flowing salt diverts around Minibasin 3, being funnelled into two fast-flowing salt streams (Fig. 6a) (*sensu* Talbot and Pohjola, 2009), one to the north and one to the south (labelled X and Y on Fig. 6a). The salt stream to the north (X) is more strongly-developed and is faster-flowing than that in the south (Y), most likely due to the wider gap (and thus greater salt flux) between Minibasins 1 and 3 than between Minibasins 2 and 3 (Fig. 6a). The salt streams continue eastwards towards the relatively thin, unwelded Minibasins 4 and 5, minibasins that were initially located approximately the same distance from the western endwall. The faster-flowing salt stream behind Minibasin 4 explains why this minibasin is strongly-propelled and translates further eastwards (light-green color) than weakly-propelled Minibasin 5 (dark green to black color) (Fig. 6a). These observations suggest that how far and how fast an unwelded and otherwise unimpeded minibasin may translate during shortening is governed largely by the horizontal velocity of the salt stream that is propelling it. Fundamentally, the horizontal velocity of a salt stream is controlled by proximity to the moving endwall (a proxy for the orogenic hinterland), and the geometry of the salt flow pathways. Thus, the distribution of minibasins, their thicknesses, and the sizes of gaps between them are fundamental controls on minibasin mobility.

Translating minibasins driven by flowing salt can be impeded in a number of ways. The most obvious one is due to primary welding, but they can also be impeded by collisions with positive base-salt relief or intrasalt bodies. Evidence of translating minibasins being impeded by primary welds is shown in Model 1b where, prior to the onset of shortening, Minibasins 1 and 2 were both located the same distance from the moving endwall (Figs. 5 and 7). Minibasin 1 welded to the base-salt earlier than Minibasin 2 (as determined by a timelapse underside view of the model, and the sheared weld visible in Figure 7). We argue that this weld preferentially restricts the eastward motion of Minibasin 1, resulting in a significant deficit in translation during shortening relative to Minibasin 2 (Fig. 7). These observations suggest that as a minibasin welds to the base-salt, the increase in friction at the interface may partially or fully impede minibasin translation.

Minibasin translation may also be impeded when minibasins collide with positive base-salt relief (or other minibasins that are themselves buttressed). We examine this in Model 2, which demonstrates the buttressing effect of a plunging base-salt structural high on a linear array of minibasins (model setup outlined in Figure 5) (see also Jackson et al., 2019, and Dooley et al., 2019). As the moving endwall shortens the initial configuration and the salt is displaced eastwards, the minibasins are also mobilized, but are gradually buttressed by the plunging base-salt high.

Minibasin 1, located adjacent to the tallest portion of the base-salt high block, translates a much shorter distance than Minibasin 3, which lies adjacent to the lowest portion of the base-salt high (Fig. 8a). Thus, the greater the overlap between the base of the minibasin and the top of the base-salt high block, the more efficient the buttress is.

The presence of intrasalt sediment bodies between minibasins may impede minibasin translation in a similar way to positive base-salt relief. We explore this in Model 3, which initially consisted of a series of intrasalt and suprasalt minibasins (see model setup in Fig. 5). As the moving endwall shortens this system, salt flow propels the shallower western suprasalt minibasins toward the eastern suprasalt minibasins and intrasalt minibasins. Where intrasalt minibasins are located directly between the converging suprasalt minibasins they act as buttresses, propping apart and preventing collision and secondary welding of the suprasalt minibasins (Fig. 9). The SE Precaspian Basin (Kazakhstan) is a natural setting where this concept is proposed to have occurred (Duffy et al., 2017).

5 Minibasin Tilting During Shortening

Entire supra-salt and encased minibasins can tilt, that is, rotate around a horizontal axis. Some of the major causes of minibasin tilting include: i) regional shortening (e.g. Hudec et al., 2009; Lopez-Mir et al., 2014; Kergaravat et al., 2016; 2017; Ribes et al., 2017; Granado et al., 2018, Legeay et al., 2019); ii) asymmetric subsidence above salt of varying thickness (Dooley et al., 2019; Jackson et al., 2019); iii) progradational loading (Callot et al., 2016) iii) pivoting of minibasins after primary welding (e.g. Rowan and Weimer, 1998; Callot et al., 2016; Ge et al., 2019); and v) kinematic interactions between subsiding minibasins (Fernandez et al., 2020). For non-encased minibasins, syn-depositional tilting phases are recorded by the deposition of wedge-shaped growth packages (e.g. Rowan and Weimer, 1998, Jackson et al., 2019; Fernandez et al., 2020), whereas post-encasement tilting of minibasins occurs below the salt-sediment interface and is thus not expressed stratigraphically (Callot et al. 2016; Duffy et al., 2017; Fernandez et al. 2017). In this section our physical models show how minibasin tilts are highly spatially- and temporally-variable during shortening. We outline what key factors may influence minibasin tilting during shortening, addressing in particular the influence of pressurized salt and minibasin interactions with base-salt relief or other minibasins.

At an early stage of shortening of Model 1b, five out of the six minibasins tilt towards the moving western endwall (Fig. 10a). A cross-section taken through Minibasins 2, 3 and 4 at the end of shortening also shows consistent tilting of lower minibasin packages towards the west (Fig. 11). This systematic early tilt towards the moving endwall occurs prior to any of the six minibasins welding to the base-salt or to one another, ruling out minibasin collision or welding to base-salt as potential contributing factors (Fig. 10a). We suggest that this systematic westward tilt direction is likely a function of the moving endwall continually pumping salt eastward, a process that pressurizes salt at the eastern end of the salt basin (Fig. 10a). Minibasins tilt westwards, away from the pressurized salt (*sensu* Hudec et al., 2009; Fernandez et al., 2020) (Fig. 10a).

Minibasins in Model 1b change tilt direction as shortening strain increases (Fig. 10). An example is Minibasin 1, a minibasin that was not welded to the base-salt at the onset of shortening and does not collide with any other minibasins (Fig. 10). At relatively low strains, Minibasin 1 tilts broadly towards the moving western endwall (WNW in Fig. 10a), then displays a horizontal top surface (Fig. 10b), before eventually tilting towards the northeast at the highest shortening strain (Fig. 10c). Given the isolated nature of Minibasin 1 we suggest the likeliest causes of the changes in tilt direction are: i) the initially WNW-tilting Minibasin 1 welded to the base-salt at some point after the onset of shortening and pivoted on the primary weld (*sensu* Rowan and Weimer, 1998; Callot et al., 2016; Ge et al., 2019; Fernandez et al., 2020), with the center of mass, geometry of the primary weld, and minibasin shape favouring tilt towards the northeast; and/or ii) shortening and relative changes in the location and horizontal translation velocities of minibasins resulted in shifts in the location of pressurized salt around the minibasin through time, with the minibasin tilting away from these zones (*sensu* Hudec et al., 2009; Fernandez et al., 2020). Controls such as these are likely to be significant for any minibasin, particularly those that do not collide with other minibasins.

Minibasin tilt directions also change significantly after they collide with other minibasins (e.g. Minibasins 2 and 3, as well as Minibasins 5 and 6; Fig. 10). For example, the tilt direction of Minibasin 5 changes by almost 180° from a stage prior, but close, to the onset of collision with the initially thicker Minibasin 6 (Fig. 10a), to a late stage in the collision process (Fig. 10c). We also see that at an early stage in its collision with the initially thicker Minibasin 3, Minibasin 2 tilts southeast (Fig. 10b), whereas later in the collision process it tilts northeast (Fig 10c). We speculate that when minibasins collide, in addition to the potential for tilt changes due to pivoting on primary welds or tilting away from zones of pressurized salt, the following factors may influence minibasin tilt histories: i) whether collision was ‘head on’ or ‘glancing’ and thus the potential for minibasins to slide past, or pivot and rotate (around a vertical axis) against one another; ii) the relative horizontal translation velocities of the minibasins; iii) the relative sizes of the minibasins; iv) the thickness of salt underlying the minibasins prior to collision; and v) changes in the location of salt streams and pressurized salt through time.

Model 2 explores how the direction and magnitude of minibasin tilting during shortening may be influenced by base-salt relief. Height-change maps illustrate how minibasins tilt away from the southward plunging high block during simple vertical loading as well as during shortening (Fig. 8b and c). Cross-sections taken through Minibasins 1, 2 and 3 at the end of shortening show each minibasin initially developed a symmetrical bowl-shaped package that is overlain by a wedge-shaped package that thickens away from the plunging high block (Fig. 8c). We interpret that minibasins tilt away from the plunging high due to the higher rate of salt flow from beneath the western flanks of the minibasins when compared to flow from beneath the eastern flanks (Fig. 8). This is a result of salt flow beneath the eastern flanks of the minibasins being restricted by the plunging base-salt high creating zones of pressurized salt (*sensu* Dooley et al., 2018, 2019; Jackson et al., 2019; Fernandez et al., 2020; Fig. 8). This sets up localized pressure gradients whereby salt preferentially flows from low pressure zones beneath the western flanks of the minibasins, driving minibasin tilt (*sensu* Fernandez et al., 2020). The transition from bowl-shaped package to wedge-shaped package in cross-section marks the onset of asymmetrical salt flow from beneath the minibasins during the vertical loading stage as the subsiding minibasin was more impacted by the base-salt high block (Fig. 8b-c). During shortening this was enhanced as the minibasins were pushed up and onto the base-salt high block. The cross-sections also show where the base-salt high is lower, the magnitude of tilt away from the high is greater (Fig. 8b), where the minibasins were forced up and onto the high block, locally enhancing the tilt (Fig. 8c).

Overall, for minibasins surrounded by salt (i.e. not welded to the base-salt or colliding with other minibasins), tilt changes are likely driven by changes in the locations of pressurized salt, a factor which may be modified by shortening-induced salt flow or effects of base-salt relief (*sensu* Hudec et al., 2009; Jackson et al., 2019; Fernandez et al., 2020). Once minibasins weld to the base-salt or collide with other minibasins, pivoting on primary and secondary welds become significant influences.

6 Minibasin Rotation Around Vertical Axes During Shortening

Model 3 shows that minibasins can rotate around vertical axes during shortening (Figs 5 and 12) (see physical modelling movies in Dooley, 2020). Strikingly, all suprasalt minibasins in Model 3 rotate significantly, with a component of rotation occurring before suprasalt minibasins welded to the base-salt (or edge of salt) or collided with other minibasins, and a component of rotation occurring afterwards (Figs. 12-14). Why do minibasins rotate prior to welding? A likely cause of rotation is evident in Figures 13 and 14a, as the amount of rotation of SMBs 1, 3 and 5 shown largely accrued prior to welding. In these figures salt streams are developed in the lowest portion of the salt (and thus detected by the DIC technique). These streams vary markedly in extent and horizontal velocity, with the difference likely related to the size of the gap between the western proximal suprasalt minibasins and/or the edge of salt (Figs. 13 and 14a). We propose that differences in the horizontal velocities of salt streams exert different degrees of traction on different parts of the outer minibasin surface. This will generate sub-vertical shear on minibasin margins and promote rotation (Figs. 13 and 14a). This concept is best-illustrated, albeit simplistically, by suprasalt Minibasin 1, which has a narrow gap between itself and the edge of salt to its north, and a wider gap between itself and suprasalt Minibasin 3 (Fig. 14a). The wider gap between suprasalt minibasin 1 and suprasalt Minibasin 3 facilitates a greater flow of salt, and thus a wider and faster-flowing salt stream than between suprasalt minibasin 1 and the northern edge of salt (Fig. 14a). These differences in the horizontal velocities of salt streams to the north and south of suprasalt Minibasin 1 generate sub-vertical shear on the minibasin boundary, driving anticlockwise rotation of suprasalt Minibasin 1 (Fig. 14a). However, such logic does not apply to many of the other suprasalt minibasins. We suggest this is a function of the 3-D nature of both salt flow and the outer surfaces of the minibasins, as well as limitations of our experimental approach. Salt streams captured on the underside of the model by the digital image correlation (DIC) technology (Figs. 13 and 14) are processed entirely in 2D and may only be showing flow patterns only in the lowest portion of the salt. In reality, these flows will vary upwards in width and horizontal velocity due to upwards changes in: i) geometry of the minibasins and thus width of the stream; and ii) the relative effect of drag from the top and base of the salt. To accurately constrain the sub-vertical shear imparted on a minibasin and test if differential traction exerted by salt streams on the resulting minibasin rotation we need a high resolution map of the 3-D distribution of traction exerted on the outer surface of the minibasin. We do not have this data available. However, we believe the concept outlined here provides the basis for testing in future physics-based numerical models..

Minibasins also rotate as they collide and pivot against other minibasins or against the edge of salt. For example, at intermediate-to-high shortening strains in Model 3, the suprasalt minibasins collide with intrasalt minibasins in various styles and influence minibasin rotation (Fig. 14). A good example is intrasalt Minibasin 5, which prior to shortening was welded to the base-salt and also located close to the southern edge of salt (Figs. 5 and 12). A shortening ensues, suprasalt Minibasin 5 translates eastward and collides with the northwestern portion of intrasalt Minibasin 5. This off-center collision and continued eastward translation of suprasalt Minibasin 5, in combination with intrasalt Minibasin 5 becoming pinned to the edge of the salt, facilitates significant clockwise rotation of intrasalt Minibasin 5 as it is pushed eastwards (Fig. 12b). We suggest that the direction, amount and speed at which minibasins rotate after collision is controlled by factors that include: i) the angle and force of collision; ii) the morphology of minibasin collision surfaces; iii) the presence, location and extent of primary welds; iv) the direction and speed of any rotation occurring prior to collision; v) the number of minibasins involved; and vi) whether a minibasin is pinned against the edge of salt. We also expect that the effect of differences in the horizontal velocity of salt streams will also exert sub-vertical shear on minibasin surfaces and promote minibasin rotation even after primary welding or collision with another minibasin. We suggest that many of the factors outlined here apply and influence minibasin rotation when large-scale supra-salt minibasins collide in nature (e.g. Rowan and Vendeville, 2006). These influences are summarized in Figure 15.

7 Discussion

7.1. Conceptual Models of Shortening in Isolated-Minibasin Provinces

Based on observations from our physical models and existing literature, we now present 3D conceptual models that summarise how, why and where many of the key processes and structural styles occur as an isolated-minibasin province shortens (Fig. 16). As in our physical models, these conceptual models focus on the thin-skinned component of shortening, with shortening propagating from the hinterland on the right. We assume the rate of salt rise due to shortening is balanced by the rate of syn-kinematic sedimentation and erosion of the minibasins, such that the top model surface remains essentially flat and no salt canopies, encased minibasins, or diapir roofs form (other model assumptions outlined in Figure caption).

Prior to shortening, minibasin subsidence was largely symmetrical, being dominated by bowl-shaped stratigraphic units (Fig. 16a). The exception is Minibasin 7, which shows a wedge-shaped unit that represents a phase of asymmetrical subsidence developed as the minibasin tilted away from the underlying base-salt high and towards the thicker salt in its foreland (Fig. 16a) (Dooley et al., 2019; Jackson et al., 2019). The only driver of salt flow prior to shortening is therefore minibasin subsidence.

At low shortening strains, shortening-induced regional salt flow propels minibasins toward the foreland, with translation of minibasins closer to the hinterland generally initiated before those in the foreland (Fig. 16b). Salt streams of locally high horizontal salt flow velocity form where salt flows through gaps between minibasins. Locally high degrees of minibasin translation are expected ahead of those streams. The net effect of these processes is that minibasins converge and the intervening salt thickens (diapir rise). In some cases, such as near the hinterland, minibasins collide, unless propped apart by base-salt relief or encased minibasins. Early stages of shortening may see minibasins preferentially tilt towards the hinterland (away from the zone of pressurized salt at the eastern edge of the model (*sensu* Fernandez et al., 2020)), although these tilts may be modified by interactions with base-salt relief or adjacent minibasins. At low strains, many salt walls remain open, particularly those aligned broadly parallel to shortening; as a result, many salt flow pathways remain open. Sub-vertical shearing imparted by variations in the horizontal velocity and direction of salt streams is therefore a likely cause of minibasin rotation, along with pivoting on any primary and secondary welds. Some minibasins may experience horizontal translation, tilting and rotation simultaneously.

At high shortening strains, most minibasins will have collided with one or more adjacent minibasins resulting in a complex map-view distribution of secondary welds, thrusts and subvertical shear zones (with components of strike-slip, reverse, and normal displacement) (Fig. 16c). Minibasins welded to the base-salt at lower strains continued to translate, shearing the primary welds. If the shortening strains and induced salt flow are sufficient, some minibasins aligned in the shortening direction and that shared a secondary weld, may translate as a single body, much as that seen in our Model 1b (Figure 11). Secondary welds oriented broadly perpendicular to the shortening direction can be preferentially transformed into thrust welds. These welds, in combination with the buttressing effects of base-salt relief, drive extreme minibasin tilting. In general, minibasin tilt directions are likely largely governed by the angle of contact and relative force of minibasin collisions, with primary welds acting as pivots. In contrast to the lower strain scenario, the dominant driver of rotation is the relative angle and force of minibasin collisions.

7.2. Influence of Precursor Salt Volume and Distribution on Fold-and-Thrust Belt Characteristics

We now synthesise how variations in precursor salt volume and distribution can influence how fold-and-thrust belts develop (Fig. 17). Of particular interest here are the striking differences between shortened isolated-diapir and shortened isolated minibasin provinces (*cf*. this paper and Duffy et al., 2018). Of these initial configurations that contain structured salt, isolated-minibasin provinces contain the highest volume of precursor salt. This higher salt volume results in a system with the lowest mechanical rigidity, the most independently-mobile minibasins, and overall, a different shortening style to isolated-diapir systems (Fig. 17).

One of the distinguishing characteristics of isolated-minibasin systems is that even at moderate shortening strains, shortening is cryptic, being accommodated by salt flow and thickening. As such, unless a thin roof records any deformation, detecting shortening or unravelling the original pre-shortening configuration of minibasins is more difficult than in squeezed isolated-diapir systems, where the surrounding sediments visibly shorten (Fig. 17; e.g. Callot et al., 2007; Dooley et al., 2009). Detecting shortening at higher strains is possible as minibasins collide and may over- and under-thrust one another and giving rise to degrees of minibasin tilt (e.g. Duffy et al., 2017; Legeay et al., 2019; Figure 16c). A second difference is that during shortening of isolated-minibasin provinces, deformation is accommodated either by salt flow and thickening, or one or a combination of translation, tilt (in a variety of directions), or rotation of entire minibasins. Minibasins, although dynamic and interacting with other minibasins, may thus remain internally-undeformed, a feature that is uncommon in shortened isolated-diapir systems (*cf*. Gottschalk et al., 2004; Callot et al., 2007; Dooley et al., 2009; Kergaravat et al., 2016; 2017; Duffy et al., 2017, 2018; Ribes et al., 2017; Granado et al., 2018; Legeay et al., 2019). A third difference is that thrust axes and welds do not form relatively continuous trends oriented broadly perpendicular (with some deviations) to the regional shortening direction as is typical of shortened isolated-diapir provinces (e.g. Fars Province of Zagros fold-and-thrust belt [e.g. Callot et al., 2007]) or even shortened areas of undeformed salt (e.g. Jura Mountains [e.g. Laubscher, 1961]). Instead, the orientations and extents of thrust axes and welds are highly-variable, being controlled by the shape and disposition of the minibasins and how they have fitted together (Figs. 16 and 17).

We recognise that the high volume of salt in shortened isolated-minibasin provinces leads to structural processes and styles that differ dramatically from what is classically considered a 'fold-and-thrust belt'. However, we argue here it appropriate to classify shortened isolated-minibasin provinces as 'fold-and-thrust belts' as: i) at high shortening strains, minibasins can over- and under-thrust one another; and ii) in natural isolated minibasin systems, it is likely there will be a thin roof over precursor diapirs that may form local contractional features.

7.3. Complex Patterns in Natural Fold-and-Thrust Belts

The pre-shortening salt volumes and configurations we have described (undeformed salt, isolated-diapir, and isolated-minibasin), represent schematic end-member scenarios intended to aid understanding of the different mechanical behaviors that govern salt-influenced fold-and-thrust-belt evolution (see companion paper by Duffy et al., 2018). We stress that many natural fold-and-thrust-belts that develop with structured precursor salt may lie on the continuum between isolated-minibasin and isolated-diapir scenarios, showing elements of shortening styles associated with both. A good example is the egg-carton-like precursor salt geometry common in the sub-canopy system of the northern Gulf of Mexico (e.g. Rowan and Vendeville, 2006). Here, isolated diapirs were connected at depth by salt anticlines that radiated out, and plunged away from the diapirs, forming a polygonal network (Rowan and Vendeville, 2006). When shortened, the system behaved partly as a relatively mechanically-rigid isolated-diapir system, with: i) salt predominantly extruded from the tallest diapirs located at triple junctions; and ii) variations in shortening styles between diapirs at triple junctions and above the more deeply anticlines (Rowan and Vendeville, 2006). However, the system also displays elements that suggest it behaved partly as an isolated-minibasin system, with shortening focused on a polygonal diapir network and evidence of independently-mobile and rotated minibasins (Rowan and Vendeville, 2006).

When applying the concepts outlined in this paper and Duffy et al. (2018) to natural examples, note that the volume and distribution of precursor salt that influenced a fold-and-thrust-belt may vary spatially and temporally within a given basin. For example, the Sivas Basin, Turkey is interpreted to have had thinner, undeformed salt in its Western Domain based on the presence of a simple fold-and-thrust belt characterised by linear folds and thrusts striking perpendicular to the regional shortening direction (Kergaravat et al., 2016; Legeay et al., 2019). In contrast, its Central Domain contains many tightly-packed, welded minibasins, some with extreme tilts, and thus consisted of isolated minibasins prior to shortening (Fig. 4c and d) (Kergaravat et al., 2016; Legeay et al., 2019).

A second example is the sub-canopy region of the salt-stock-canopy province in the lower-slope of the northern Gulf of Mexico. This area has experienced protracted shortening in the contractional domain of a gravity-driven slope system detached on the autochthonous Louann salt (e.g. Diegel et al., 1995; Peel et al., 1995; Rowan et al., 1999; Pilcher et al., 2011; Dooley et al., 2013). Fiduk et al (2016) (their Figure 4) present a regional base salt canopy map that shows isolated diapirs surrounded by a rigid, continuous sediment body, that is, an isolated-diapir scenario, in the centre-south region. In contrast, in the northeast, more diapirs are present in the form of partially-connected linear walls. This configuration is a hybrid of the isolated-minibasin and isolated-diapir scenarios. Thus, different parts of the same basin contain different salt volumes and distributions, a factor that may result in different mechanical responses to lateral shortening, and different fold-and-thrust belt geometries.

Natural fold-and-thrust belts may also contain multiple detachment levels as a result of canopy development (e.g. Sivas Basin, Turkey [e.g. Ringenbach et al., 2013; Callot et al., 2014; Kergaravat et al., 2016; 2017; Ribes et al., 2017; Legeay et al., 2019]; northern Gulf of Mexico, USA [Diegel et al., 1995; Peel et al., 1995]; Axel-Heiberg Island, Artic Canada [Harrison and Jackson, 2014]) or due to the occurrence of different weak (detachment) layers in the deformed section (e.g. Zagros fold-and-thrust belt, Iran [Sherkati and Letouzey, 2004; Verges et al., 2011; Najafi et al., 2014; Ghanadian et al., 2017; Hassanpour et al., 2020]). Duffy et al (2020) show an example from the mid-lower slope region of the northern Gulf of Mexico (their Figure 4), where the sub-canopy consists of isolated feeders (isolated-diapir scenario). In contrast, above the canopy, isolated minibasins are adrift in the Sigsbee salt canopy (isolated-minibasin scenario). In such systems, shortening associated with different detachment levels may thus affect different precursor salt volumes and configurations, and shortening styles may vary significantly between deep and shallow systems. This concept is highlighted by the different shortening styles that occur above and below the allochthonous salt in the Betics (e.g. Flinch and Soto, 2017).

8 Summary

This study has used observations from natural salt-influenced fold-and-thrust belts and a suite of new physical models to examine the processes and structural styles that occur in shortened isolated-minibasin provinces. Our key findings are:

- When shortening occurs, the weak salt localizes contractional strain and the strong, mobile minibasins move independently of one another. Shortening in isolated-minibasins provinces may therefore be hard to detect, particularly at low shortening strains, as shortening is primarily accommodated by salt inflation. This means that minibasin thickness is not a proxy for original salt thickness in shortened isolated-minibasin provinces.

- As weak salt localizes contraction strain it induces salt flow, in some cases in highly-localized streams of high horizontal velocities. This flowing salt around minibasins propels them in the direction of shortening. Several factors can restrict the translation of minibasins during shortening: i) the presence of relatively thin salt below the minibasin; ii) friction associated with primary welding; and iii) collision and buttressing effects of base-salt relief, intrasalt bodies or intrasalt minibasins.

- Isolated minibasins commonly tilt during shortening, with the direction and magnitude of tilt being highly spatially and temporally-variable. In our models, minibasins tend to tilt gently toward the shortening direction at low strains, which we attribute here to being a result of differential salt pressure within the basin. A regionally-consistent tilt direction may therefore indicate shortening, but this tilt may be modified or even reversed by: i) asymmetric subsidence associated with structure or relief at base salt; ii) pivoting on primary welds; iii) minibasin collision; and iv) tilt away from other localized zones of pressurized salt. Tilts can become extreme at high shortening strains, facilitated by minibasin collision, thrusted secondary welds, and the buttressing effect of base-salt relief.

- Minibasins can rotate around vertical axes to significant degrees during shortening. In the absence of welding and/or collision with other minibasins or base-salt relief, minibasin rotation is likely caused by sub-vertical shearing imparted on the minibasin boundary by variations in the horizontal velocity and direction of salt streams in 4D. Variations in horizontal flow velocities of streams are likely to develop as a result of the local geometry and configuration of minibasins (note that our minibasins are circular in planform), the edges of the salt basin, and the local dip. Once minibasins weld to the base-salt, or collide with base-salt relief, intrasalt bodies or the edge of the salt basin, they may rotate as they jostle with and pivot against these features, likely aided by continued flow-induced shearing.

- The kinematics of minibasins in shortening isolated-minibasin systems may be complex and highly-variable both spatially and temporally. Minibasins may experience varying degrees and rates of translation, tilt and rotation; in some circumstances these processes may occur independently, but in others they may occur simultaneously. The extent to which the different processes affect a minibasin is likely dependent on factors that amongst others includes: tectonic boundary conditions; the size, geometry and spatial configuration of minibasins; the thickness of salt underlying minibasins; and the nature of local base-salt relief.

By placing the findings of this paper into context with those of companion paper Duffy et al (2018), we conclude that differences in the volume and distribution of salt prior to shortening result in different kinematic processes and structural styles in the subsequent fold-and-thrust belts. In particular, kinematic processes and structural styles vary markedly between settings where precursor salt is in flat-bedded, isolated-diapir, or isolated-minibasin end-member configurations, respectively. These end-member settings differ in terms of: i) thrust style and evolution; ii) map-view configuration of faults and welds; iii) degree of internal deformation within the minibasins;

iv) minibasin mobility: v) the degree to which shortening may be accommodated by cryptic deformation. We also note how natural fold-and-thrust-belts have developed with precursor salt volumes and distributions that were hybrids of the end-member scenarios examined in the pair of papers. Furthermore, basins may show spatial variations in precursor salt volume and distribution, and this may also vary through time.

9 Acknowledgements

We would like to thank Nancy Cottington for figure drafting. We thank Martin Jackson, Gillian Apps, Frank Peel, and Mark Rowan for scientific discussions. The project was funded by the Applied Geodynamics Laboratory (AGL) Industrial Associates program, comprising the following companies: Anadarko, Aramco Services, BHP Billiton, BP, CGG, Chevron, Condor, EcoPetrol, EMGS, ENI, ExxonMobil, Hess, Ion-GXT, Midland Valley, Murphy, Nexen USA, Noble, Petrobras, Petronas, PGS, Repsol, Rockfield, Shell, Spectrum, Equinor, Stone Energy, TGS, Total, WesternGeco, and Woodside (http://www.beg.utexas.edu/agl/sponsors). The authors received additional support from the Jackson School of Geosciences, The University of Texas at Austin. Publication authorised by the Director, Bureau of Economic Geology, The University of Texas at Austin. The authors confirm no conflicts of interest.

10 Data Availability Statement

The physical modelling movies that support the findings of this study are openly available in Figshare at https://figshare.com/account/articles/12659828

11 Figure Captions

Figure 1. Schematic diagrams showing a pre-shortening configuration typical of a) an 'isolated-diapir province' and b) an 'isolated-minibasin' province. In a) salt makes up a low proportion of the rock volume and is distributed in discrete salt stocks and walls. In b) salt makes up a higher proportion of the rock volume and forms a connected network of diapirs that surround isolated minibasins. The strength of any diapir roof stratigraphy is assumed to be negligible.

Figure 2. The style of shortening that occur in salt provinces is strongly influenced by whether or not diapirs were present prior to the onset of shortening. These forward models maintain salt area through time (after Hudec and Jackson, 2007).

Figure 3. Maps showing the top of salt (silicone polymer) at different stages of a physical modelling experiment into shortening of a system where the pre-shortening salt distribution and volume was broadly analogous to an isolated-minibasin setting (Fig. 1b): (a) pre-shortening configuration and (b) after shortening. In a) minibasins are separated by a polygonal network of deep salt ridges, with shallow diapirs typically located at the ridge triple junctions. In the strictest sense, our definition of the isolated-minibasin end member, the deep salt ridges would extend upwards to more fully-isolate each minibasin (see section 7.3). In b) diapirs and the ridges accommodate shortening and minibasins translate and interact with other minibasins. Redrawn and modified from Rowan and Vendeville (2006).

Figure 4. Map and section views showing general characteristics of some natural shortened isolated-minibasin provinces. (a) Structure map of the Top Kungurian Salt from a portion of the mildly-shortened SE Precaspian Basin (Kazakhstan). Structural lows host isolated minibasins that are surrounded by a polygonal network of diapirs (modified from Fernandez et al. [2017]). (b) geoseismic section taken along the kinked black and white line in a) that shows the main structural elements of the area. Note the tilting of the supra-salt minibasin fill (modified from Duffy et al. [2017]). c) Simplified geological map of the highly-shortened central portion of the Sivas Basin showing the distribution of minibasins (blue), salt (red), and key structural features. Note how minibasins are isolated from one another, being surrounded on all sides by salt or an equivalent weld. Map modified from Kergaravat et al. (2016) and incorporating key data from Kurtman (1973), Guezou et al. (1996), and Poisson et al. (1996). d) Cross-section along Line X-X' in c) (parallel to shortening direction) showing a tectonic wedge with thrusts in sub-evaporite strata, and two generations of supra-salt minibasins separated by an evaporite canopy or an equivalent tertiary? weld. Note: i) the marked variations in tilts of the minibasins, some are flat-lying whereas others are highly-upturned; and ii) the tight-packing of internally-undeformed minibasins. Pairs of black dots mark welds. Redrawn from Kergaravat et al. (2016).

Figure 5. Chart summarizing the design and parameters used for the physical models presented in the text. Models are numbered in the order they are introduced in the text. SMB = suprsasalt minibasin. IMB = intrasalt minibasin.

Figure 6. Maps showing the shortening-parallel (eastward) displacement on the top surface of Model 1a (calculated over a period of one minibasin sand fill cycle) at: a) 4.5 cm cumulative shortening; and b) 16.5 cm cumulative shortening. Warmer colours equal more eastward movement. X and Y are salt streams that are flowing eastwards and propelling the eastward translation of Minibasins 4 and 5 respectively.

Figure 7. Underside view of Model 1b at the end of shortening. Minibasin 1, which welded to the base salt earlier than Minibasin 2 has translated a shorter distance eastwards indicating that primary welding impedes minibasin translation. The white line A-B shows the line of section of the SW-NE-oriented cross-section shown in Figure 11.

Figure 8. Outputs from Model 2. a) on left is the overhead view at the start of the model run and on the bottom is a schematic view of the degree of overlap between the base of the minibasins and the top of the plunging high prior to the onset of shortening. On the right is an overhead view during shortening showing the shortening-parallel (eastward) displacement on the top surface of Model 2 (calculated over a period of one minibasin sand fill cycle). Warmer colours represent faster eastward-moving salt streams. b) views of the height change of top salt surface during the vertical subsidence stage (left) and during shortening (right). Note the marked tilt of minibasins towards the moving endwall (west) in both stages. c) W-E-oriented cross-sections through each minibasin at the end of shortening. Note the westward-thickening growth wedges and the tilting of the lower section of the minibasins towards the west. All minibasins have translated eastwards and welded onto the plunging high. Minibasins located adjacent to where the top of the plunging high is deeper (i.e. less of a barrier) translate further eastwards.

Figure 9. Outputs from Model 3. a) cross-section views at the end of shortening (location of sections shown in (b)), and b) underside view of Model 3 at end of shortening. Where one or more intrasalt minibasins (IMB's) are located directly between the converging suprasalt minibasins (SMB's) they act as buttresses, propping apart and preventing collision and secondary welding of the suprasalt minibasins.

Figure 10. Overhead views showing height change maps (calculated over a period of one minibasin sand fill cycle) that illustrate the translation and tilt changes that occur as Model 1b shortens at: a) 4.5 cm shortening, b) 16.5 cm shortening, and c). 19.5 cm shortening. Note the collision of minibasins and the marked spatial and temporal variation in tilt magnitude and direction as the model shortens.

Figure 11. SW-NE-oriented cross-section taken through supra-salt minibasins 2, 3 and 4 (oblique to shortening) at the end of shortening of Model 1b. Growth wedges immediately above the first blue unit indicate consistent early tilt of minibasins towards the moving endwall. Location of section shown by line A-B on Fig 7.

Figure 12. Underside views of Model 3 at a) 16 cm (intermediate shortening strain) and b) 31 cm shortening (high shortening strain). a) Suprasalt minibasins 1, 3 and 5 rotate prior to forming primary or secondary welds. b) Minibasins can also rotate after forming primary or secondary welds, pivoting on the welds (including with the edge of the salt basin). Intrasalt minibasins prevent the collision of suprasalt minibasins during shortening.

Figure 13. Underside views of Model 3 at early stages of shortening showing the shortening-parallel (eastward) displacement at the model base (calculated over a period of one minibasin sand fill cycle). Note the gradual anticlockwise rotation of SMB 3. Small white arrows are vectors of movement and indicate rotation. Note the development of salt streams between the minibasins.

Figure 14. Underside views of Model 3 showing the shortening-parallel (eastward) displacement at the model base at: a) 8 cm shortening, and b) 17 cm shortening. Vector arrows indicate rotation of minibasins. Some rotations occurred before minibasins welded to the base salt formed secondary welds (e.g. SMB 3) or, and some occurred afterwards.

Figure 15. Map-view schematic model showing: i) some of the key drivers of minibasin rotation; and ii) some common interactions between supra-salt and intra-salt minibasins, that occur as an isolated-minibasin provinces shortens. Rotations around vertical axes are driven by variations in the magnitude, horizontal velocity and direction of salt flow as a result of: i) the local configuration of minibasins and intra-salt bodies; and ii) pivoting against other minibasins, base-salt relief or the edge of salt. Red = mobile salt. Grey = non-salt, immobile rocks.

Figure 16. 3-D conceptual block models synthesising the structural styles and processes that occur in isolated-minibasin provinces as they shorten. a) pre-shortening configuration. b) low shortening strain. c) high shortening strain. The model is based on a system with a single generation of minibasins, with no salt canopies, and, with the exception of a single base-salt high, the base-salt is flat. We assume minibasins are largely unwelded to the base-salt prior to shortening, but as shortening ensues more minibasins ground to form primary welds – a scenario that ensures the widest range of structural styles and processes are captured in the conceptual model. We also assume flow perturbations related to minibasin subsidence were of insufficient scale to modify the subsidence patterns of adjacent minibasins (*cf.* Fernandez et al., 2020).

Figure 17. Schematic comparison of the key characteristics of fold-and-thrust-belts developed with different precursor volumes and and distributions of salt: a) flat, undeformed salt; b) an isolated-diapir scenario (*sensu* Duffy et al., 2018); and c) an isolated-minibasin scenario (this paper). a) shows a relatively simple set of folds and thrusts striking perpendicular to the shortening direction and that are continuous along-strike. b) weak diapirs localize contractional strain and are squeezed. Faults and folds nucleate at diapirs, propagate out into the surrounding sedimentary rocks and link with those from adjacent diapirs. Folds and thrusts are not continuous along-strike, instead they deviate to link up precursor diapirs. There are marked along-strike variations in structural style; welds, squeezed diapirs and thrusted welds at diapirs, compared to folds and thrusts in the intervening sedimentary rocks. c) minibasins are independently-mobile and experience translation, tilting and rotation as they are propelled by flowing salt during shorteninig and collide with one another. Folds and thrusts may be highly-discontinuous and show highly-variable strikes. These factors are governed by the shape of minibasins and the angle of collisions between minibasins.

11 References

Adam, J., Urai, J., Wieneke, B., Oncken, O., Pfeiffer, K., Kukowski, N., Lohrmann, J., Hoth, S., Van Der Zee, W. & Schmatz, J. (2005) Shear Localisation and Strain Distribution During Tectonic Faulting—New Insights from Granular-Flow Experiments and High-Resolution Optical Image Correlation Techniques. *Journal of Structural Geology*, **27,** 283-301.

Baby, P., Calderón, Y., Brusset, S., Roddaz, M., Brichau, S., Eude, A., Calves, G., Calderón, Y., Quispe, A. & Ramirez, L. (2018) The Peruvian Sub-Andean Foreland Basin System: Structural Overview, Geochronologic Constraints, and Unexplored Plays. *Aapg Memoirs, Petroleum basins and hydrocarbon potential of the Andes of Peru and Bolivia*, **117**, 91-120.

Butler, R.W. (2019) Syn-Kinematic Strata Influence the Structural Evolution of Emergent Fold–Thrust Belts. *Geological Society, London, Special Publications*, **490,** SP490-2019-2014.

Callot, J.P., Jahani, S. & Letouzey, J. (2007) The Role of Pre-Existing Diapirs in Fold and Thrust Belt Development. In: *Thrust Belts and Foreland Basins*, 309-325. Springer.

Callot, J.P., Trocme, V., Letouzey, J., Albouy, E., Jahani, S. & Sherkati, S. (2012) Pre-Existing Salt Structures and the Folding of the Zagros Mountains. *Salt Tectonics, Sediments and Prospectivity*, **363,** 545-561.

Callot, J.P., Ribes, C., Kergaravat, C., Bonnel, C., Temiz, H., Poisson, A., Vrielynck, B., Salel, J.F. & Ringenbach, J.C. (2014) Salt Tectonics in the Sivas Basin (Turkey): Crossing Salt Walls and Minibasins. *Bulletin De La Societe Geologique De France*, **185,** 33-42.

Callot, J.P., Salel, J.F., Letouzey, J., Daniel, J.M. & Ringenbach, J.C. (2016) Three-Dimensional Evolution of Salt-Controlled Minibasins: Interactions, Folding, and Megaflap Development. *Aapg Bulletin*, **100,** 1419-1442.

Costa, E. & Vendeville, B.C. (2002) Experimental Insights on the Geometry and Kinematics of Fold-and-Thrust Belts above Weak, Viscous Evaporitic Decollement. *Journal of Structural Geology*, **24,** 1729-1739.

Cotton, J.T. & Koyi, H.A. (2000) Modeling of Thrust Fronts above Ductile and Frictional Detachments: Application to Structures in the Salt Range and Potwar Plateau, Pakistan. *Geological Society of America Bulletin*, **112,** 351-363.

Darnault, R., Callot, J.P., Ballard, J.F., Fraisse, G., Mengus, J.M. & Ringenbach, J.C. (2016) Control of Syntectonic Erosion and Sedimentation on Kinematic Evolution of a Multidecollement Fold and Thrust Zone: Analogue Modeling of Folding in the Southern Subandean of Bolivia. *Journal of Structural Geology*, **89,** 30-43.

Davis, D.M. & Engelder, T. (1985) The Role of Salt in Fold-and-Thrust Belts. *Tectonophysics*, **119,** 67-88.

Diegel, F.A., Karlo, J., Schuster, D., Shoup, R. & Tauvers, P. (1995) Cenozoic Structural Evolution and Tectono-Stratigraphic Framework of the Northern Gulf Coast Continental Margin. *Aapg Memoirs, Salt Tectonics: A Global Perspective*, **65**, 109-151.

Dooley, T.P., Jackson, M.P.A. & Hudec, M.R. (2007) Initiation and Growth of Salt-Based Thrust Belts on Passive Margins: Results from Physical Models. *Basin Research*, **19,** 165-177.

Dooley, T.P., Jackson, M.P.A. & Hudec, M.R. (2009) Inflation and Deflation of Deeply Buried Salt Stocks During Lateral Shortening. *Journal of Structural Geology*, **31,** 582-600.

Dooley, T.P., Jackson, M.P. & Hudec, M.R. (2013) Coeval Extension and Shortening above and Below Salt Canopies on an Uplifted, Continental Margin: Application to the Northern Gulf of Mexico. *AAPG bulletin*, **97,** 1737-1764.

Dooley, T.P., Jackson, M.P.A. & Hudec, M.R. (2015) Breakout of Squeezed Stocks: Dispersal of Roof Fragments, Source of Extrusive Salt and Interaction with Regional Thrust Faults. *Basin Research*, **27,** 3-25.

Dooley, T.P. (2020) Physical Models - Shortening of Isolated-Minibasin Provinces https://figshare.com/account/articles/12659828

Duffy, O.B., Fernandez, N., Hudec, M.R., Jackson, M.P.A., Burg, G., Dooley, T.P. & Jackson, C.A.L. (2017) Lateral Mobility of Minibasins During Shortening: Insights from the Se Precaspian Basin, Kazakhstan. *Journal of Structural Geology*, **97,** 257-276.

Duffy, O.B., Dooley, T.P., Hudec, M.R., Jackson, M.P.A., Fernandez, N., Jackson, C.A.L. & Soto, J.I. (2018) Structural Evolution of Salt-Influenced Fold-and-Thrust Belts: A Synthesis and New Insights from Basins Containing Isolated Salt Diapirs. *Journal of Structural Geology*, **114,** 206-221.

Duffy, O.B., Fernandez, N., Peel, F.J., Hudec, M.R., Dooley, T.P. & Jackson, C.A.L. (2020) Obstructed Minibasins on a Salt-Detached Slope: An Example from above the Sigsbee Canopy, Northern Gulf of Mexico. *Basin Research*. **32 (3),** 505-524.

Fernandez, N., Duffy, O.B., Hudec, M.R., Jackson, M.P.A., Burg, G., Jackson, C.A.L. & Dooley, T.P. (2017) The Origin of Salt-Encased Sediment Packages: Observations from the Se Precaspian Basin (Kazakhstan). *Journal of Structural Geology*, **97,** 237-256.

Fernandez, N., Hudec, M.R., Jackson, C.A.-L., Dooley, T.P. & Duffy, O.B. (2020) The Competition for Salt and Kinematic Interactions between Minibasins During Density-Driven Subsidence: Observations from Numerical Models. *Petroleum Geoscience*, **26,** 3-15.

Fiduk, J.C., Robertson, V., Clippard, M., Jamieson, G.A. & Power, S. (2016) Extensional Salt Keels Detached on Eocene-Oligocene Sediments in the Deepwater Northern Gulf of Mexico: Insights into Canopy Advancement, Salt-Sediment Interplay, and Evidence for Unrecognized Mass Sediment Displacement. *GCAGS Journal*, 5, 47–63.

Flinch, J.F. & Soto, J.I. (2017) Allochthonous Triassic and Salt Tectonic Processes in the Betic-Rif Orogenic Arc. In: *Permo-Triassic Salt Provinces of Europe, North Africa and the Atlantic Margins*, 417-446. Elsevier.

Fort, X., Brun, J.P. & Chauvel, F. (2004) Salt Tectonics on the Angolan Margin, Synsedimentary Deformation Processes. *Aapg Bulletin*, **88,** 1523-1544.

Frey, M.G. (1973) Influence of Salina Salt on Structure in New-York-Pennsylvania Part of Appalachian-Plateau. *American Association of Petroleum Geologists Bulletin*, **57,** 1027-1037.

Ge, Z.Y., Gawthorpe, R.L., Rotevatn, A., Zijerveld, L., Jackson, C.A.L. & Oluboyo, A. (2019) Minibasin Depocentre Migration During Diachronous Salt Welding, Offshore Angola. *Basin Research*.

Ghanadian, M., Faghih, A., Fard, I.A., Kusky, T. & Maleki, M. (2017) On the Role of Incompetent Strata in the Structural Evolution of the Zagros Fold-Thrust Belt, Dezful Embayment, Iran. *Marine and Petroleum Geology*, **81,** 320-333.

Granado, P., Roca, E., Strauss, P., Pelz, K. & Muñoz, J.A. (2018) Structural Styles in Fold-and-Thrust Belts Involving Early Salt Structures: The Northern Calcareous Alps (Austria). *Geology*, **47 (1),** 51-54.

Grelaud, S., Sassi, W., de Lamotte, D.F., Jaswal, T. & Roure, F. (2002) Kinematics of Eastern Salt Range and South Potwar Basin (Pakistan): A New Scenario. *Marine and Petroleum Geology*, **19,** 1127-1139.

Guellec, S., Lajat, D., Mascle, A., Roure, F. & Tardy, M. (1990) Deep Seismic Profiling and Petroleum Potential in the Western Alps - Constraints with Ecors Data, Balanced Cross-Sections and Hydrocarbon Modeling. *Potential of Deep Seismic Profiling for Hydrocarbon Exploration*, **48,** 425-437.

Guezou, J.-C., Temiz, H., Poisson, A. & Gürsoy, H. (1996) Tectonics of the Sivas Basin: The Neogene Record of the Anatolian Accretion Along the Inner Tauric Suture. *International Geology Review*, **38,** 901-925.

Harrison, J.C. & Jackson, M.P.A. (2014) Exposed Evaporite Diapirs and Minibasins above a Canopy in Central Sverdrup Basin, Axel Heiberg Island, Arctic Canada. *Basin Research*, **26,** 567-596.

Hassanpour, J., Yassaghi, A., Muñoz, J.A. & Jahani, S. (2020) Salt Tectonics in a Double Salt-Source Layer Setting (Eastern Persian Gulf, Iran): Insights from Interpretation of Seismic Profiles and Sequential Cross-Section Restoration. *Basin Research*.

Hermoza, W., Brusset, S., Baby, P., Gil, W., Roddaz, M., Guerrero, N. & Bolaños, R. (2005) The Huallaga Foreland Basin Evolution: Thrust Propagation in a Deltaic Environment, Northern Peruvian Andes. *Journal of South American Earth Sciences*, **19,** 21-34.

Hudec, M.R. & Jackson, M.P. (2007) Terra Infirma: Understanding Salt Tectonics. *Earth-Science Reviews*, **82,** 1-28.

Jackson, M.P. & Hudec, M.R. (2017) *Salt Tectonics: Principles and Practice*. Cambridge University Press.

Jackson, C.A.L., Duffy, O.B., Fernandez, N., Dooley, T.P., Hudec, M.R., Jackson, M.P. & Burg, G. (2019) The Stratigraphic Record of Minibasin Subsidence, Precaspian Basin, Kazakhstan. *Basin Research*.

Kergaravat, C., Ribes, C., Legeay, E., Callot, J.P., Kavak, K.S. & Ringenbach, J.C. (2016) Minibasins and Salt Canopy in Foreland Fold-and-Thrust Belts: The Central Sivas Basin, Turkey. *Tectonics*, **35,** 1342-1366.

Kergaravat, C., Ribes, C., Callot, J.P. & Ringenbach, J.C. (2017) Tectono-Stratigraphic Evolution of Salt-Controlled Minibasins in a Fold and Thrust Belt, the Oligo-Miocene Central Sivas Basin. *Journal of Structural Geology*, **102,** 75-97.

Krantz, R.W. (1991) Measurements of Friction Coefficients and Cohesion for Faulting and Fault Reactivation in Laboratory Models Using Sand and Sand Mixtures. *Tectonophysics*, **188,** 203-207.

Kurtman, F. (1973) Sivas-Hafik-Zara Ve Imranli Bölgesinin Jeolojik Ve Tektonik Yapisi. *Bull. General Directorate of Mineral Research and Exploration of Turkey*, **80,** 1-32.

Lacombe, O. & Bellahsen, N. (2016) Thick-Skinned Tectonics and Basement-Involved Fold-Thrust Belts: Insights from Selected Cenozoic Orogens. *Geological Magazine*, **153,** 763-810.

Laubscher, H.P. (1961) Die Fernschubhypothese Der Jurafaltung. *Eclogae Geologicae Helvetiae*, **54,** 222-282.

Legeay, E., Ringenbach, J.-C., Kergaravat, C., Pichat, A., Mohn, G., Vergés, J., Kavak, K.S. & Callot, J.-P. (2019) Structure and Kinematics of the Central Sivas Basin (Turkey): Salt Deposition and Tectonics in an Evolving Fold-and-Thrust Belt. *Geological Society, London, Special Publications*, **490,** SP490-2019-2092.

Leitner, C. & Spötl, C. (2017) The Eastern Alps: Multistage Development of Extremely Deformed Evaporites. In: *Permo-Triassic Salt Provinces of Europe, North Africa and the Atlantic Margins*, 467-482. Elsevier.

Letouzey, J., Colletta, B., Vially, R. & Chermette, J.C. (1995) Evolution of Salt-Related Structures in Compressional Settings. *Salt Tectonics: A Global Perspective*, **65,** 41-60.

Lopez-Mir, B., Munoz, J.A. & Senz, J.G. (2014) Restoration of Basins Driven by Extension and Salt Tectonics: Example from the Cotiella Basin in the Central Pyrenees. *Journal of Structural Geology*, **69,** 147-162.

McClay, K. (1990) Deformation Mechanics in Analogue Models of Extensional Fault Systems. *Geological Society, London, Special Publications*, **54,** 445-453.

McClay, K., Tamara, J., Hammerstein, J., Mora, A., Zamora, G. & Uzkeda, H. (2018) Sub-Andean Thick and Thin-Skinned Thrust Systems of Southeastern Peru and Bolivia—a Review. *Aapg Memoirs, Petroleum basins and hydrocarbon potential of the Andes of Peru and Bolivia*, **117**, 35-62.

Morley, C.K., King, R., Hillis, R., Tingay, M. & Backe, G. (2011) Deepwater Fold and Thrust Belt Classification, Tectonics, Structure and Hydrocarbon Prospectivity: A Review. *Earth-Science Reviews*, **104,** 41-91.

Najafi, M., Yassaghi, A., Bahroudi, A., Vergés, J. & Sherkati, S. (2014) Impact of the Late Triassic Dashtak Intermediate Detachment Horizon on Anticline Geometry in the Central Frontal Fars, Se Zagros Fold Belt, Iran. *Marine and petroleum geology*, **54,** 23-36.

Nilsen, K.T., Vendeville, B.C. & Johansen, J.T. (1995) Influence of Regional Tectonics on Halokinesis in the Nordkapp Basin, Barents Sea. *Salt Tectonics: A Global Perspective*, **65,** 413-436.

Peel, F.J., Travis, C.J. & Hossack, J.R. (1995) Genetic Structural Provinces and Salt Tectonics of the Cenozoic Offshore Us Gulf of Mexico: A Preliminary Analysis. *Salt Tectonics: A Global Perspective*, **65,** 153-175.

Pilcher, R.S., Kilsdonk, B. & Trude, J. (2011) Primary Basins and Their Boundaries in the Deep-Water Northern Gulf of Mexico: Origin, Trap Types, and Petroleum System Implications. *Aapg Bulletin*, **95,** 219-240.

Poisson, A., Guezou, J., Ozturk, A., Inan, S., Temiz, H., Gürsöy, H., Kavak, K.S. & Özden, S. (1996) Tectonic Setting and Evolution of the Sivas Basin, Central Anatolia, Turkey. *International Geology Review*, **38,** 838-853.

Reber, J.E., Cooke, M.L. & Dooley, T.P. (2020) What Model Material to Use? A Review on Rock Analogs for Structural Geology and Tectonics. *Earth-Science Reviews*, **202,** 103107.

Ribes, C., Kergaravat, C., Bonnel, C., Crumeyrolle, P., Callot, J.P., Poisson, A., Temiz, H. & Ringenbach, J.C. (2015) Fluvial Sedimentation in a Salt-Controlled Mini-Basin: Stratal Patterns and Facies Assemblages, Sivas Basin, Turkey. *Sedimentology*, **62,** 1513-1545.

Ribes, C., Kergaravat, C., Crumeyrolle, P., Lopez, M., Bonnel, C., Poisson, A., Kavak, K.S., Callot, J.P. & Ringenbach, J.C. (2017) Factors Controlling Stratal Pattern and Facies Distribution of Fluvio-Lacustrine Sedimentation in the Sivas Mini-Basins, Oligocene (Turkey). *Basin Research*, **29,** 596-621.

Ringenbach, J.-C., Salel, J.-F., Kergaravat, C., Ribes, C., Bonnel, C. & Callot, J.-P. (2013) Salt Tectonics in the Sivas Basin, Turkey: Outstanding Seismic Analogues from Outcrops. *first break*, **31**.

Rossi, D. & Storti, F. (2003) New Artificial Granular Materials for Analogue Laboratory Experiments: Aluminium and Siliceous Microspheres. *Journal of Structural Geology*, **25,** 1893-1899.

Rowan, M.G., Jackson, M.P. & Trudgill, B.D. (1999) Salt-Related Fault Families and Fault Welds in the Northern Gulf of Mexico. *AAPG bulletin*, **83,** 1454-1484.

Rowan, M.G. & Vendeville, B.C. (2006) Foldbelts with Early Salt Withdrawal and Diapirism: Physical Model and Examples from the Northern Gulf of Mexico and the Flinders Ranges, Australia. *Marine and Petroleum Geology*, **23,** 871-891.

Ruh, J.B., Verges, J. & Burg, J.P. (2018) Shale-Related Minibasins Atop a Massive Olistostrome in an Active Accretionary Wedge Setting: Two-Dimensional Numerical Modeling Applied to the Iranian Makran. *Geology*, **46,** 791-794.

Schellart, W. (2000) Shear Test Results for Cohesion and Friction Coefficients for Different Granular Materials: Scaling Implications for Their Usage in Analogue Modelling. *Tectonophysics*, **324,** 1-16.

Sherkati, S. & Letouzey, J. (2004) Variation of Structural Style and Basin Evolution in the Central Zagros (Izeh Zone and Dezful Embayment), Iran. *Marine and petroleum geology*, **21,** 535-554.

Sherkati, S., Letouzey, J. & de Lamotte, D.F. (2006) Central Zagros Fold-Thrust Belt (Iran): New Insights from Seismic Data, Field Observation, and Sandbox Modeling. *Tectonics*, **25**.

Snidero, M., Munoz, J.A., Carrera, N., Butille, M., Mencos, J., Motamedi, H., Piryaei, A. & Sabat, F. (2019) Temporal Evolution of the Darmadan Salt Diapir, Eastern Fars Region, Iran. *Tectonophysics*, **766,** 115-130.

Sommaruga, A., Mosar, J., Schori, M. & Gruber, M. (2017) The Role of the Triassic Evaporites Underneath the North Alpine Foreland. In: *Permo-Triassic Salt Provinces of Europe, North Africa and the Atlantic Margins*, 447-466. Elsevier.

Talbot, C.J. & Pohjola, V. (2009) Subaerial Salt Extrusions in Iran as Analogues of Ice Sheets, Streams and Glaciers. *Earth-Science Reviews*, **97,** 155-183.

Vergés, J., Goodarzi, M., Emami, H., Karpuz, R., Efstathiou, J. & Gillespie, P. (2011) Multiple Detachment Folding in Pusht-E Kuh Arc, Zagros: Role of Mechanical Stratigraphy.

Weijermars, R. (1986) Flow Behaviour and Physical Chemistry of Bouncing Putties and Related Polymers in View of Tectonic Laboratory Applications. *Tectonophysics*, **124,** 325-358.

Weijermars, R., Jackson, M.t. & Vendeville, B. (1993) Rheological and Tectonic Modeling of Salt Provinces. *Tectonophysics*, **217,** 143-174.

Figure 1

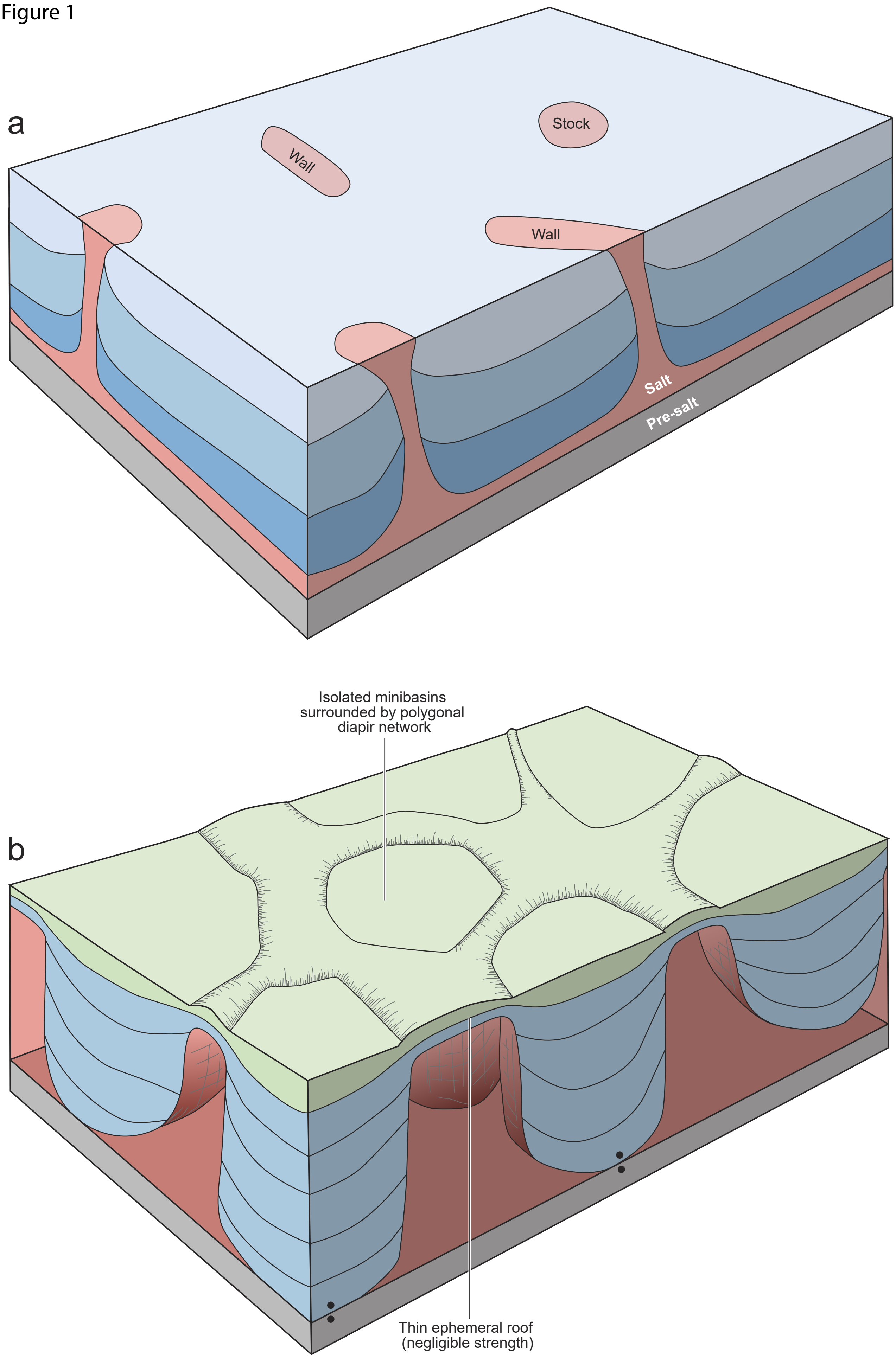
a
Stock
Wall
Wall
Salt
Pre-salt
b
Isolated minibasins
surrounded by polygonal
diapir network
Thin ephemeral roof
(negligible strength)

Figure 2

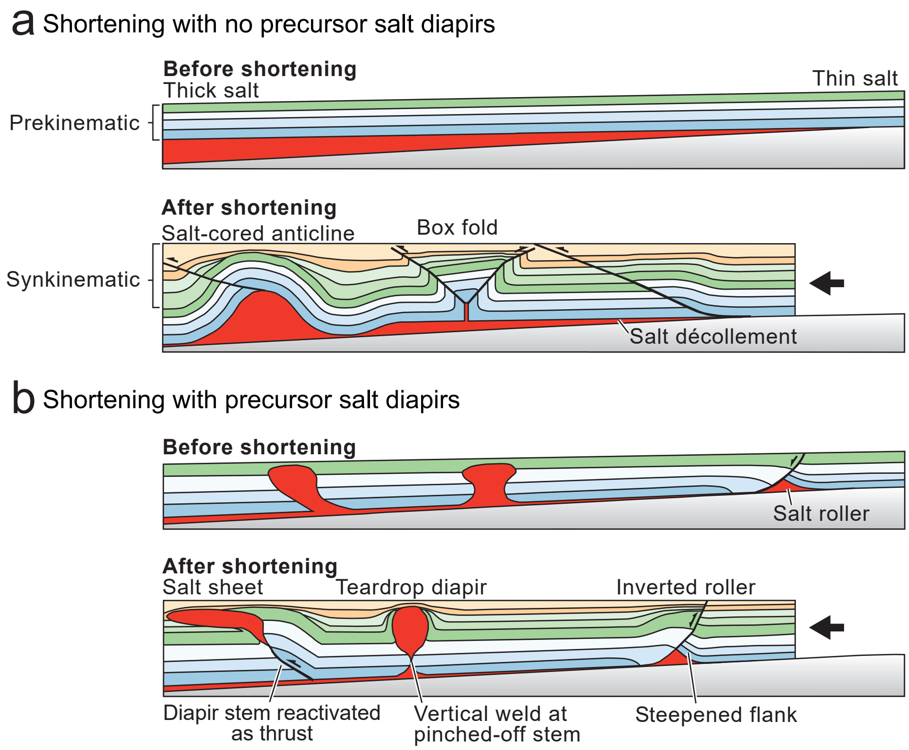
a Shortening with no precursor salt diapirs
Before shortening
Thick salt
Thin salt
Prekinematic
After shortening
Salt-cored anticline
Box fold
Synkinematic
Salt décollement
b Shortening with precursor salt diapirs
Before shortening
Salt roller
After shortening
Salt sheet
Teardrop diapir
Inverted roller
Diapir stem reactivated as thrust
Vertical weld at pinched-off stem
Steepened flank

Figure 3

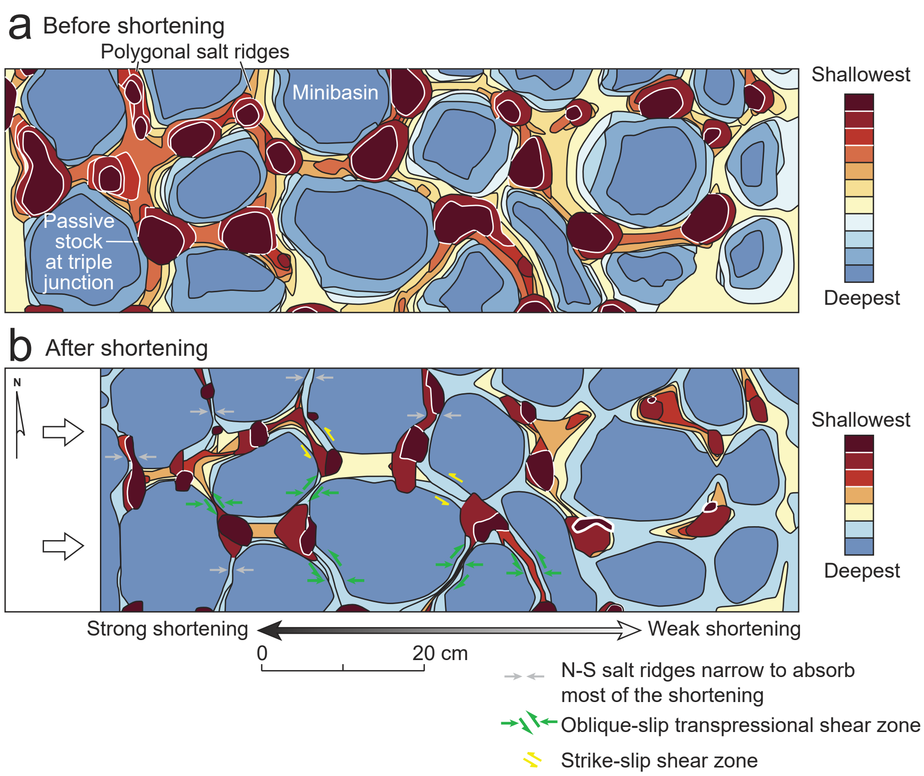
a Before shortening
Polygonal salt ridges
Minibasin
Passive stock at triple junction
Shallowest
Deepest
b After shortening
N
Shallowest
Deepest
Strong shortening
Weak shortening
0
20 cm
N-S salt ridges narrow to absorb most of the shortening
Oblique-slip transpressional shear zone
Strike-slip shear zone

Figure 4a and b

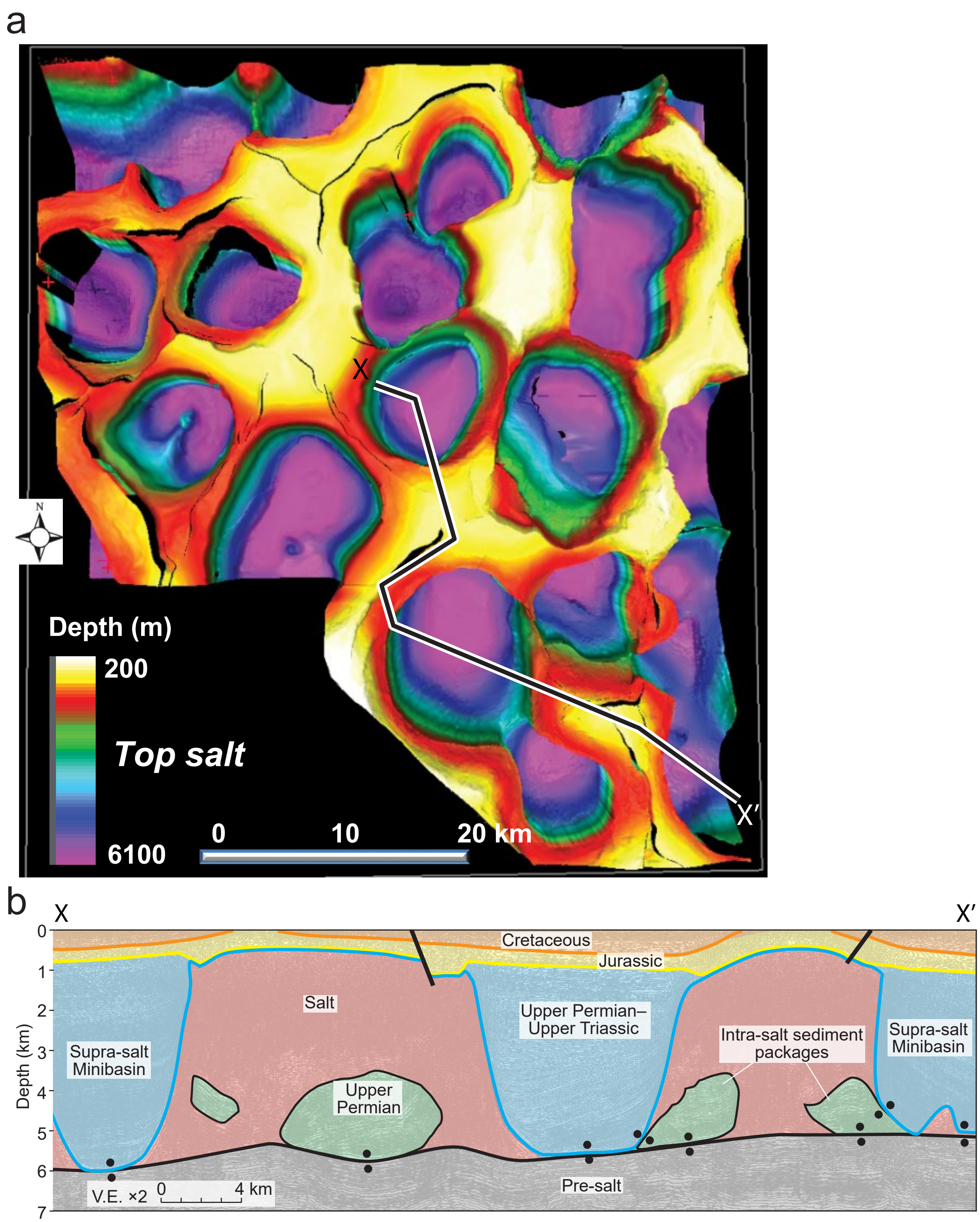

Figure 4c and d

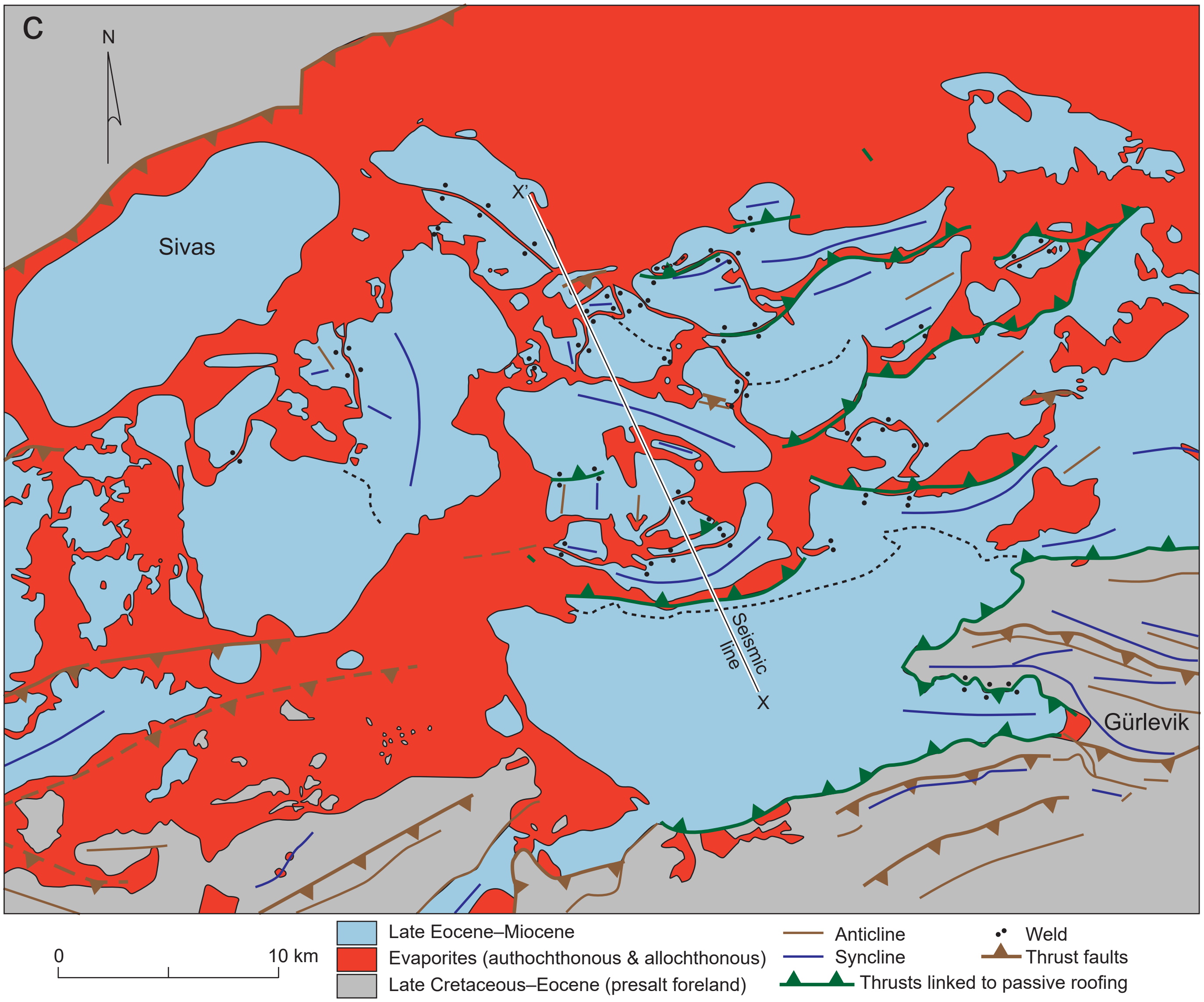

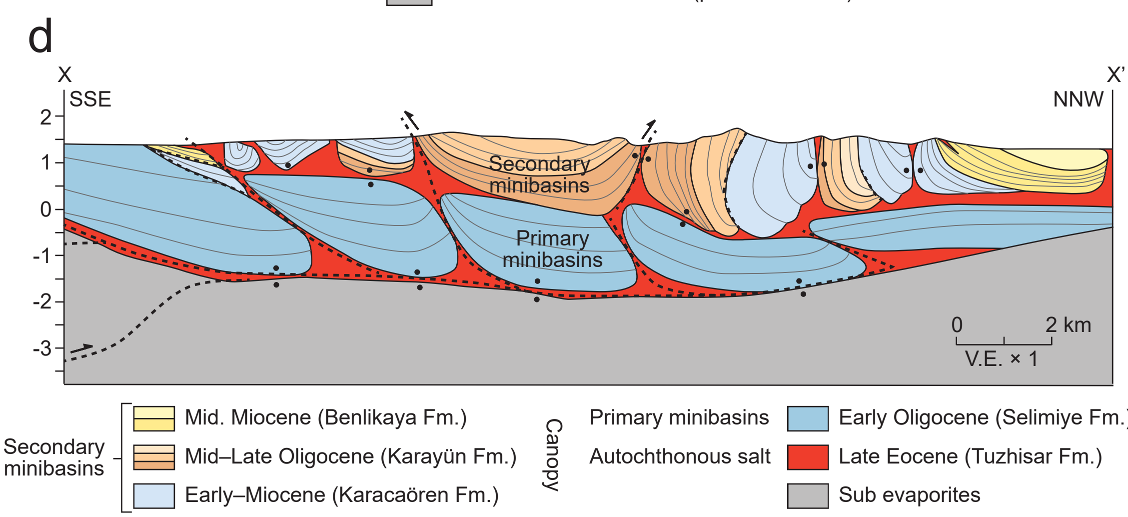

<table>
<tr><th>Model #</th><th>Regional dip</th><th>Source layer thickness</th><th>Total Shortening</th><th>Model design</th></tr>
<tr><td>Models 1a, 1b</td><td>0°</td><td>5 cm</td><td>33 cm</td><td rowspan="2">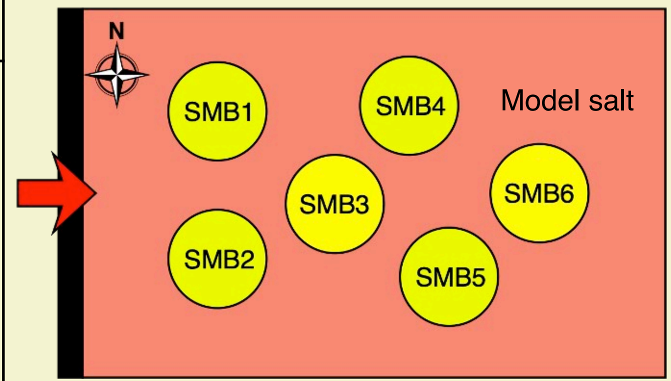
</td></tr>
<tr><td colspan="4">Model description:
6 supra salt minibasins (SMB) sunk into a 5-cm-thick salt basin. In Model 1a minibasins 3 and 6 subsided until about 1 cm from base of salt before the moving endwall began to shorten the basin. All other minibasins were 2 cm from base of salt before shortening. In Model 1b all minibasins were approximately 2 cm from base of salt before shortening was applied.

Sediments were continually added to the minibasins during shortening.</td></tr>
<tr><td>Model 2</td><td>0°</td><td>5 cm</td><td>12.5 cm</td><td rowspan="2">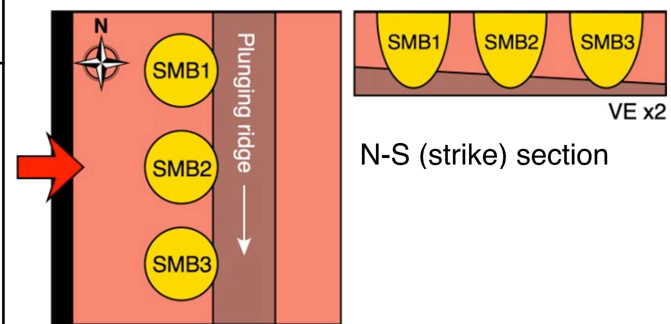
</td></tr>
<tr><td colspan="4">Model description:
3 supra salt minibasins (SMB) sunk into a 5-cm-thick salt basin. A plunging base-salt high block was located to the right of the minibasins going from 2.5 cm to 0.5 cm across the model. Once the minibasins had subsided to just 0.5 cm from welding the salt basin was shortened. Sediments were continually added to the minibasins during shortening.</td></tr>
<tr><td>Model 3</td><td>0°</td><td>5 cm</td><td>31</td><td rowspan="2">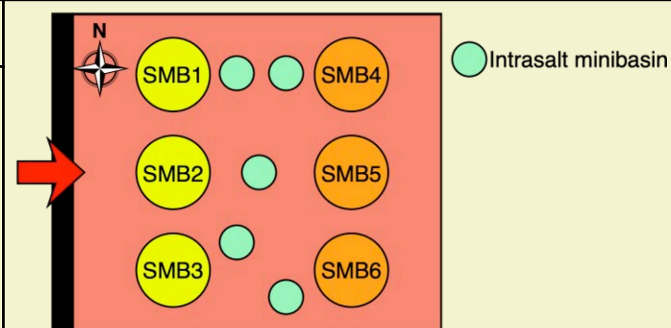
</td></tr>
<tr><td colspan="4">Model description:
5 small minibasins were sunk into a 1.5-cm-thick salt layer before being encased (IMB) in a further 3.5 cm of salt analog. 6 suprasalt minibasins (SMB) were seeded into the salt basin on either side of the intrasalt minibasin (IMB) array. Suprasalt minibasins 4-6 were sunk to where they just welded, whereas suprasalt minibasins 1-3 subsided to 2.5 cm from base of salt before shortening. Sediments were continually added to the SMBs during shortening.</td></tr>
</table>

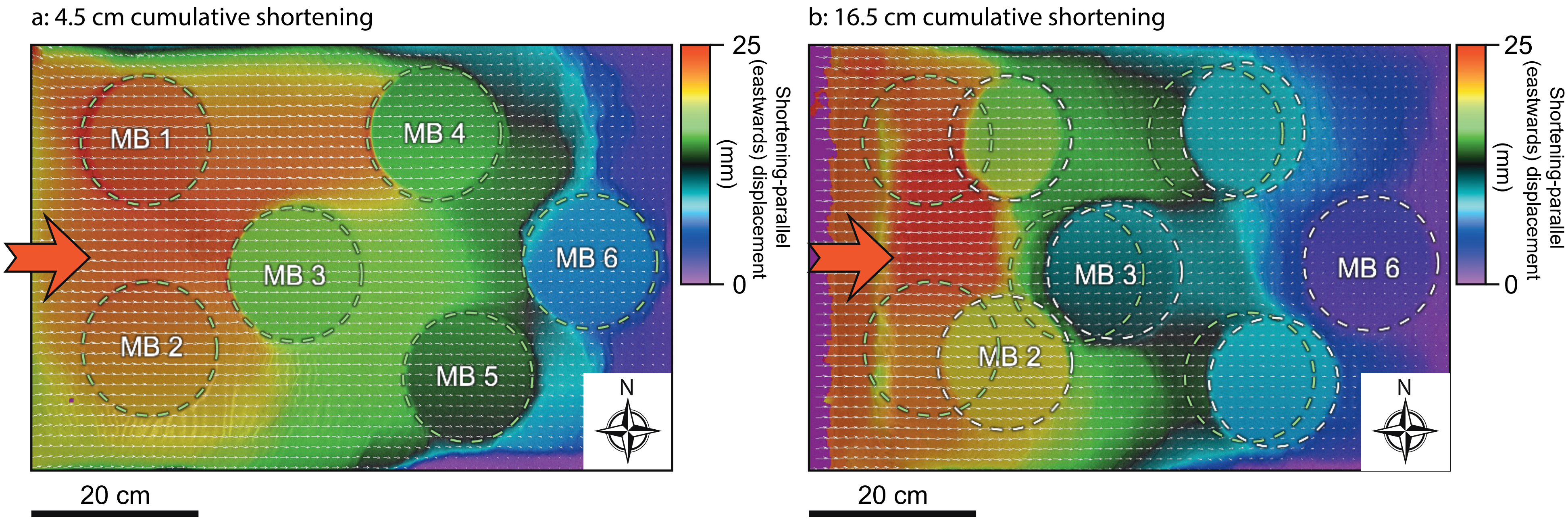

a: 4.5 cm cumulative shortening
b: 16.5 cm cumulative shortening
MB 1
MB 2
MB 3
MB 4
MB 5
MB 6
25
0
Shortening-parallel (eastwards) displacement (mm)
N
20 cm

Figure 6

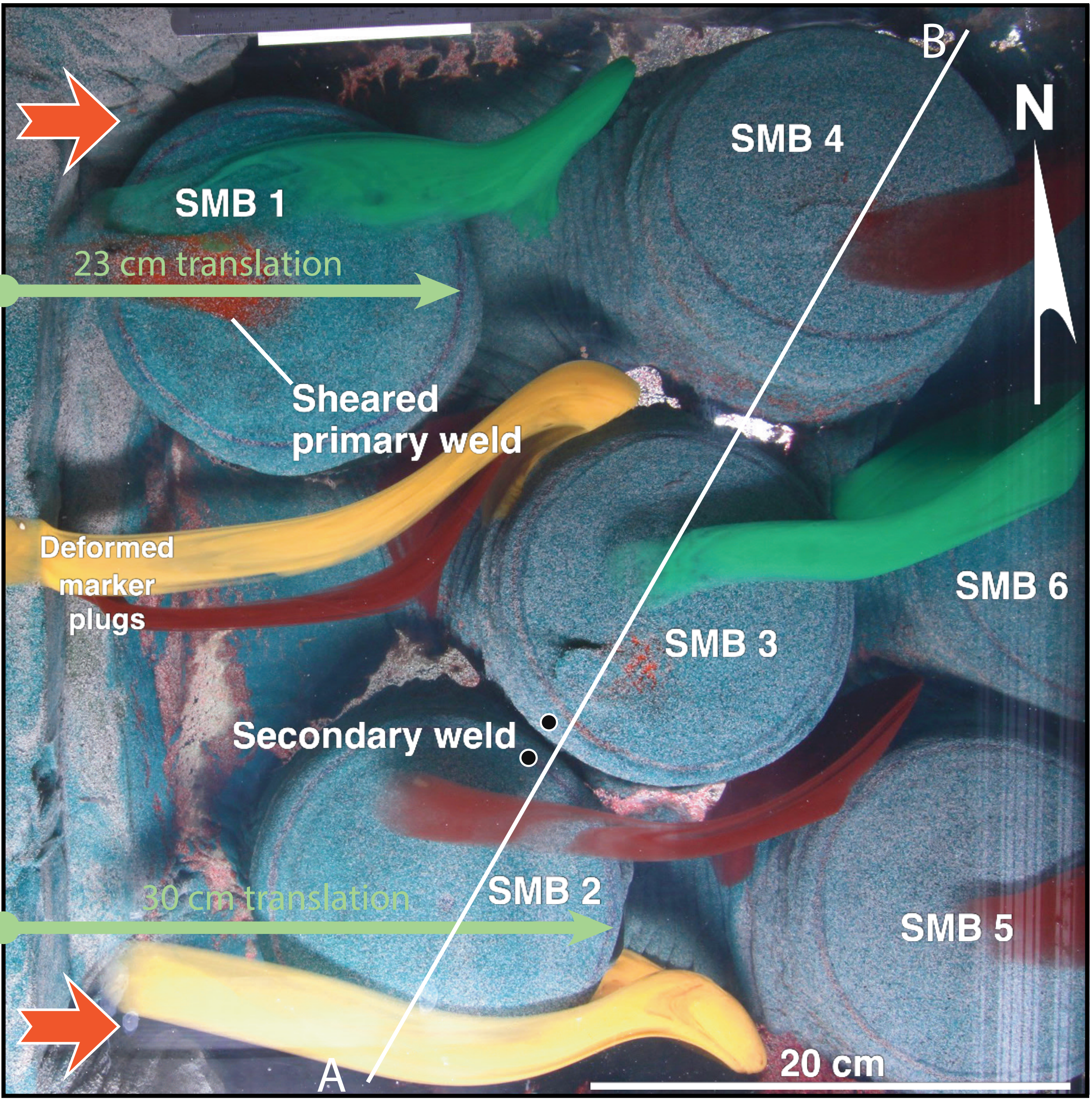

B
N
SMB 4
SMB 1
23 cm translation
Sheared
primary weld
Deformed
marker
plugs
SMB 6
SMB 3
Secondary weld
30 cm translation
SMB 2
SMB 5
20 cm
A

Figure 7

Figure 8

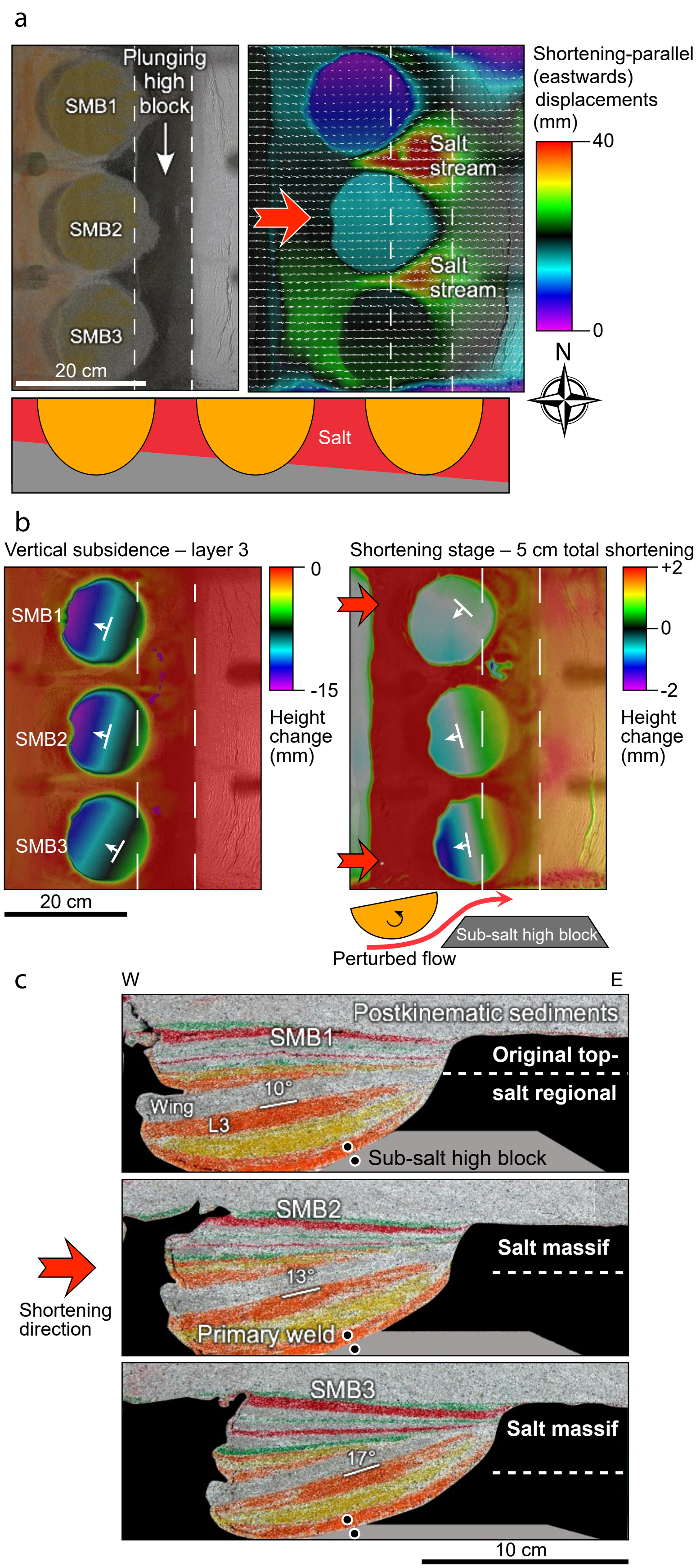

a
Plunging high block
SMB1
SMB2
SMB3
20 cm
Salt stream
Salt stream
Shortening-parallel (eastwards) displacements (mm)
40
0
N
Salt
b
Vertical subsidence – layer 3
Shortening stage – 5 cm total shortening
SMB1
SMB2
SMB3
0
-15
Height change (mm)
+2
0
-2
Height change (mm)
20 cm
Sub-salt high block
Perturbed flow
c
W
E
Postkinematic sediments
SMB1
Original top-
salt regional
10°
Wing
L3
Sub-salt high block
SMB2
Salt massif
13°
Primary weld
Shortening direction
SMB3
Salt massif
17°
10 cm

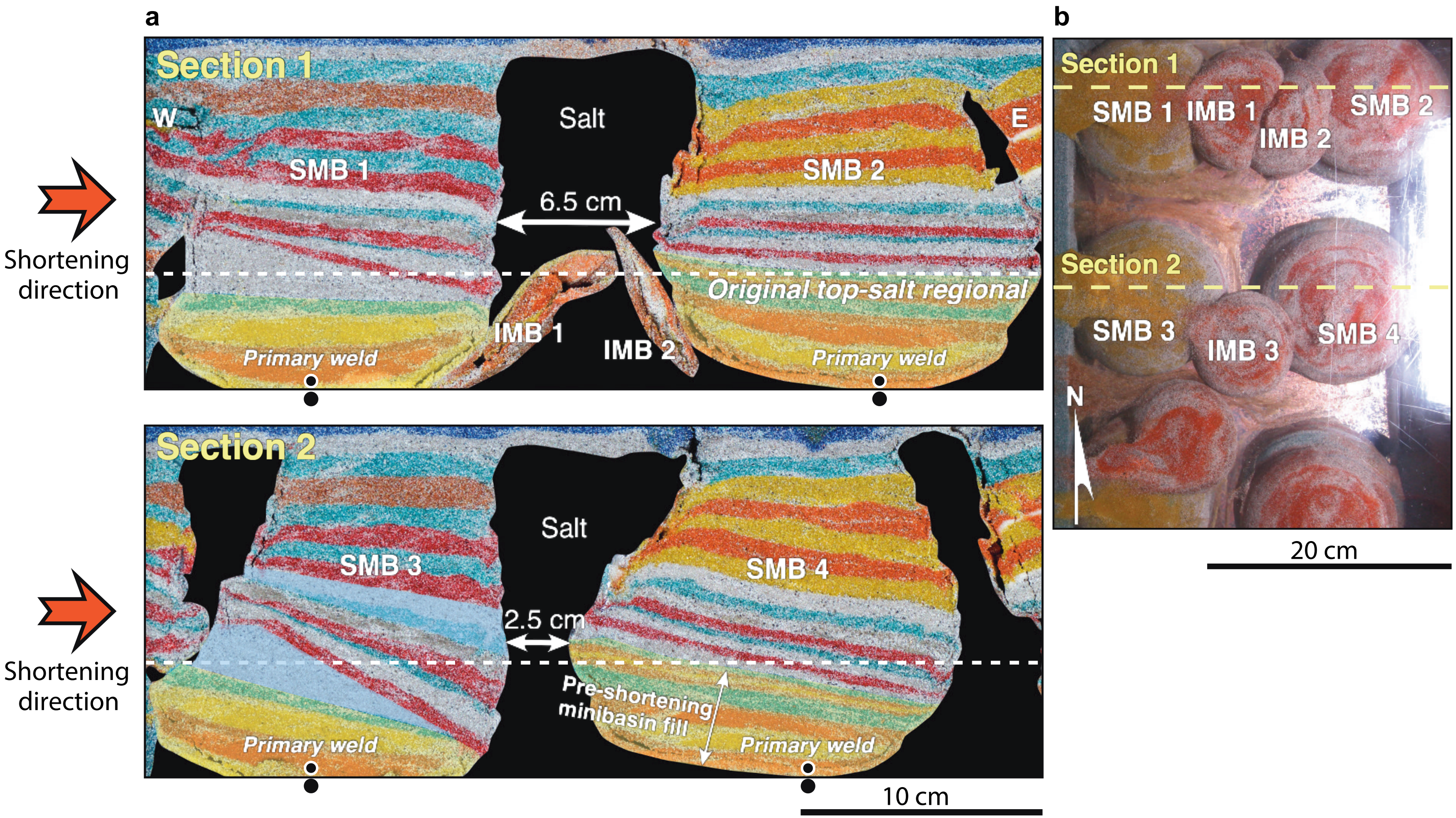
a
Section 1
W
Salt
E
SMB 1
SMB 2
6.5 cm
Original top-salt regional
IMB 1
IMB 2
Primary weld
Primary weld
Shortening direction
Section 2
Salt
SMB 3
SMB 4
2.5 cm
Pre-shortening minibasin fill
Primary weld
Primary weld
Shortening direction
10 cm
b
Section 1
SMB 1
IMB 1
IMB 2
SMB 2
Section 2
SMB 3
IMB 3
SMB 4
N
20 cm

Figure 9

Figure 10

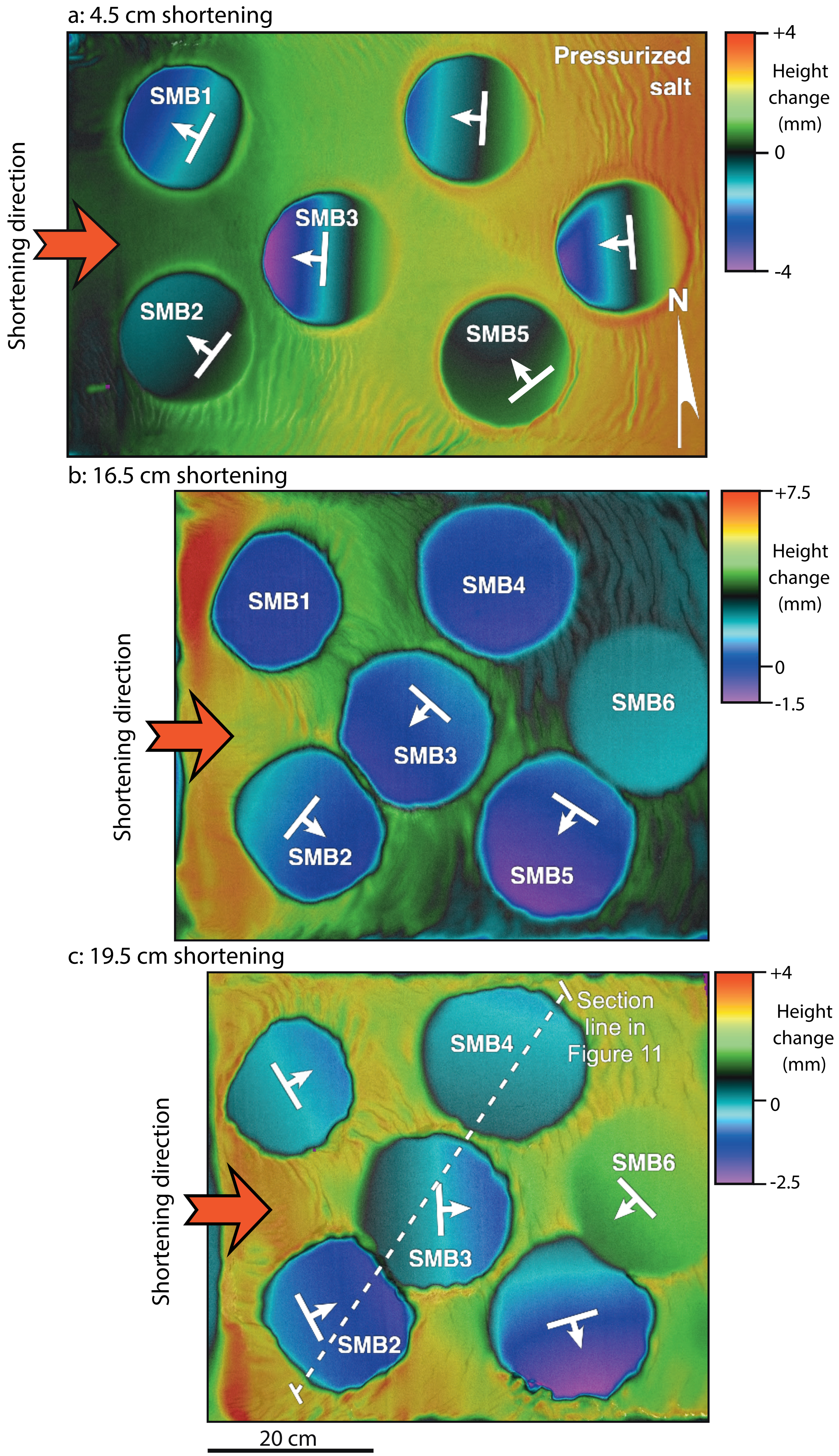
a: 4.5 cm shortening
Pressurized salt
SMB1
SMB2
SMB3
SMB5
N
Shortening direction
+4
Height change (mm)
0
-4
b: 16.5 cm shortening
SMB1
SMB2
SMB3
SMB4
SMB5
SMB6
Shortening direction
+7.5
Height change (mm)
0
-1.5
c: 19.5 cm shortening
SMB2
SMB3
SMB4
SMB6
Section line in Figure 11
Shortening direction
+4
Height change (mm)
0
-2.5
20 cm

Figure 11

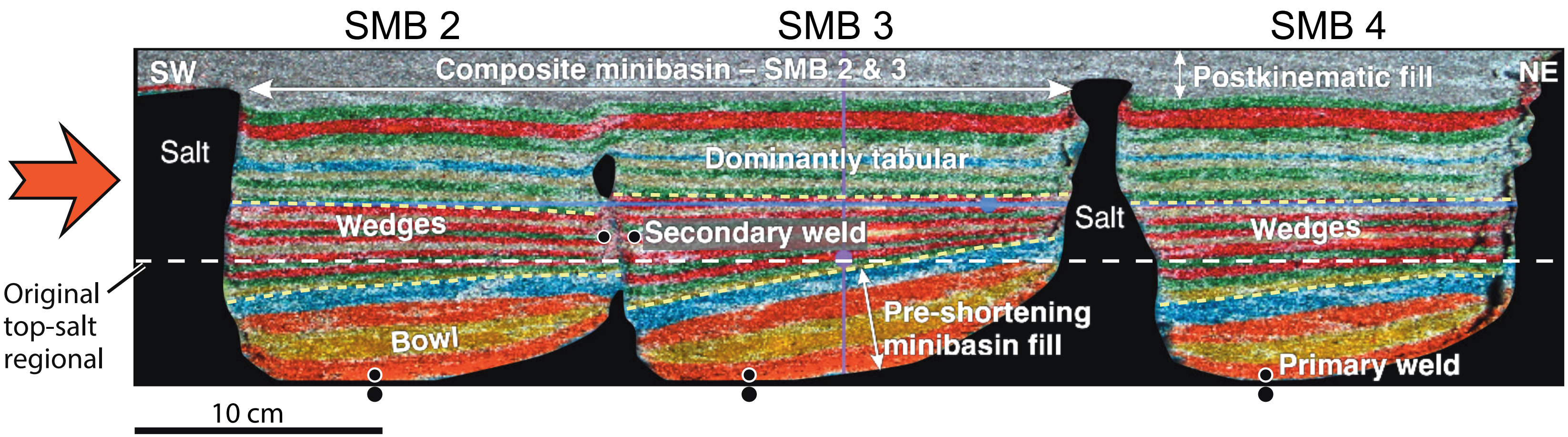
SMB 2
SMB 3
SMB 4
SW
Composite minibasin – SMB 2 & 3
Postkinematic fill
NE
Salt
Dominantly tabular
Wedges
Secondary weld
Salt
Wedges
Original top-salt regional
Pre-shortening minibasin fill
Bowl
Primary weld
10 cm

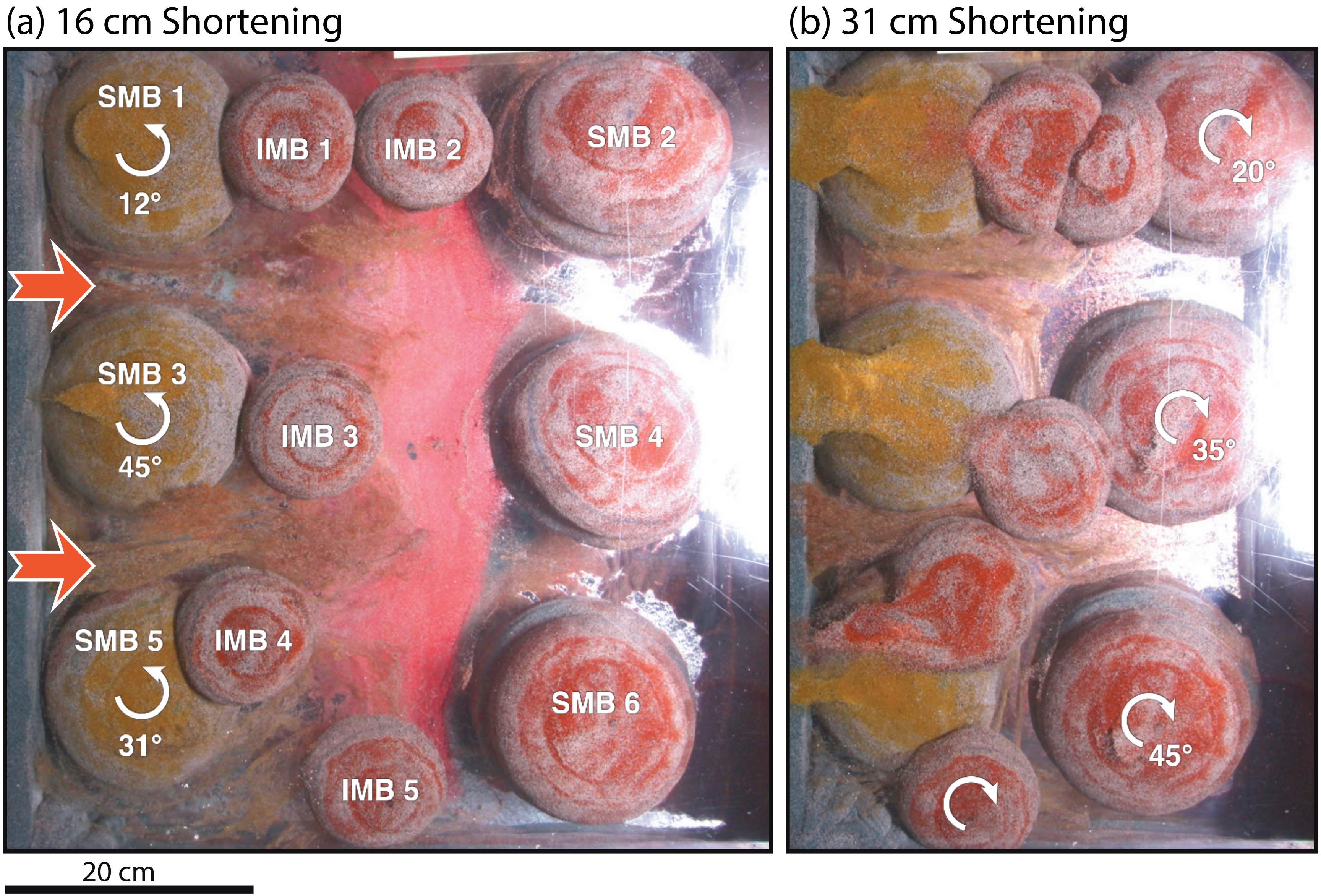

(a) 16 cm Shortening
SMB 1
12°
IMB 1
IMB 2
SMB 2
SMB 3
45°
IMB 3
SMB 4
SMB 5
31°
IMB 4
SMB 6
IMB 5
(b) 31 cm Shortening
20°
35°
45°
20 cm

Figure 12

Figure 13

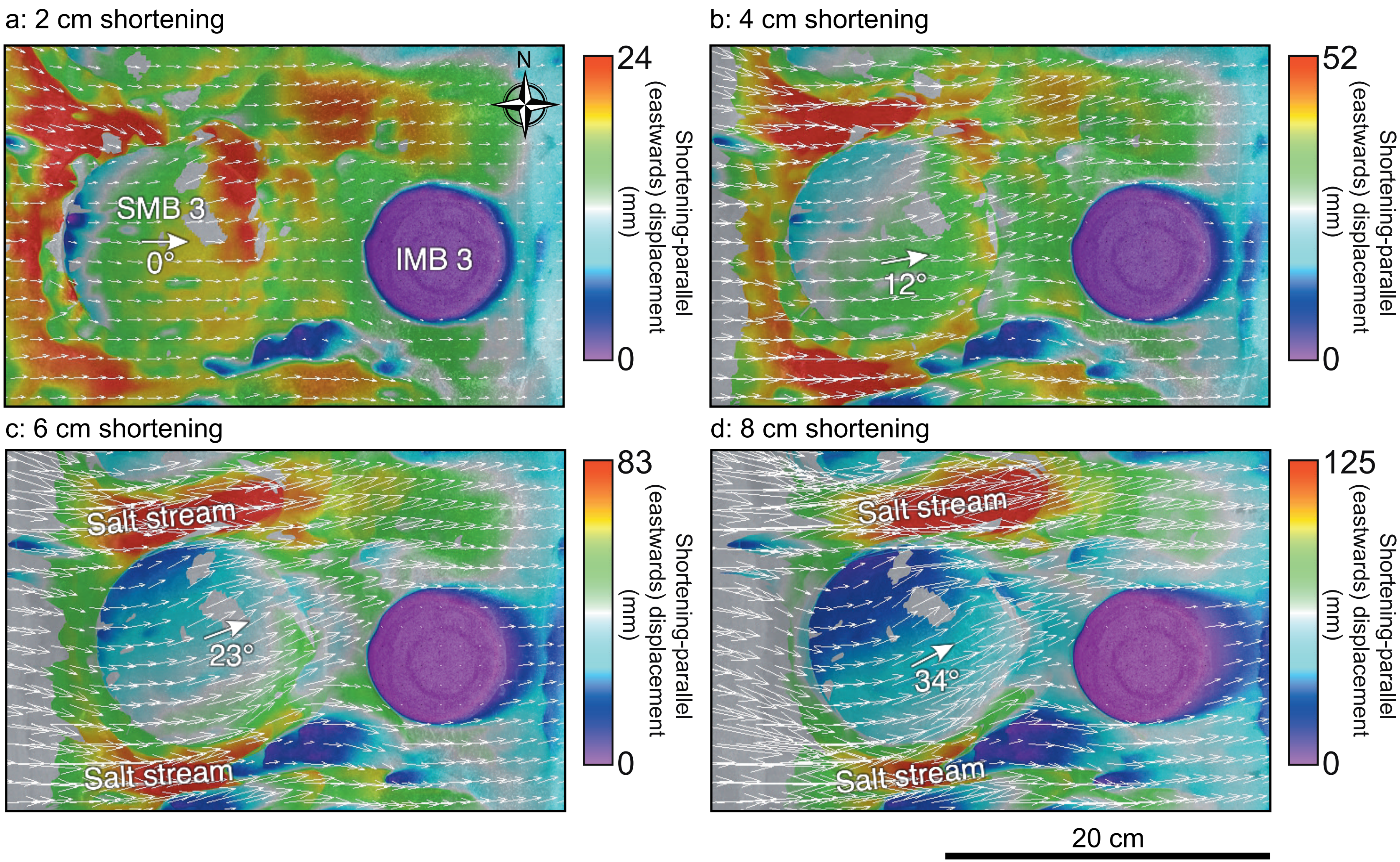

a: 2 cm shortening
N
SMB 3
0°
IMB 3
24
0
Shortening-parallel (eastwards) displacement (mm)
b: 4 cm shortening
12°
52
0
Shortening-parallel (eastwards) displacement (mm)
c: 6 cm shortening
Salt stream
23°
Salt stream
83
0
Shortening-parallel (eastwards) displacement (mm)
d: 8 cm shortening
Salt stream
34°
Salt stream
125
0
Shortening-parallel (eastwards) displacement (mm)
20 cm

Figure 14

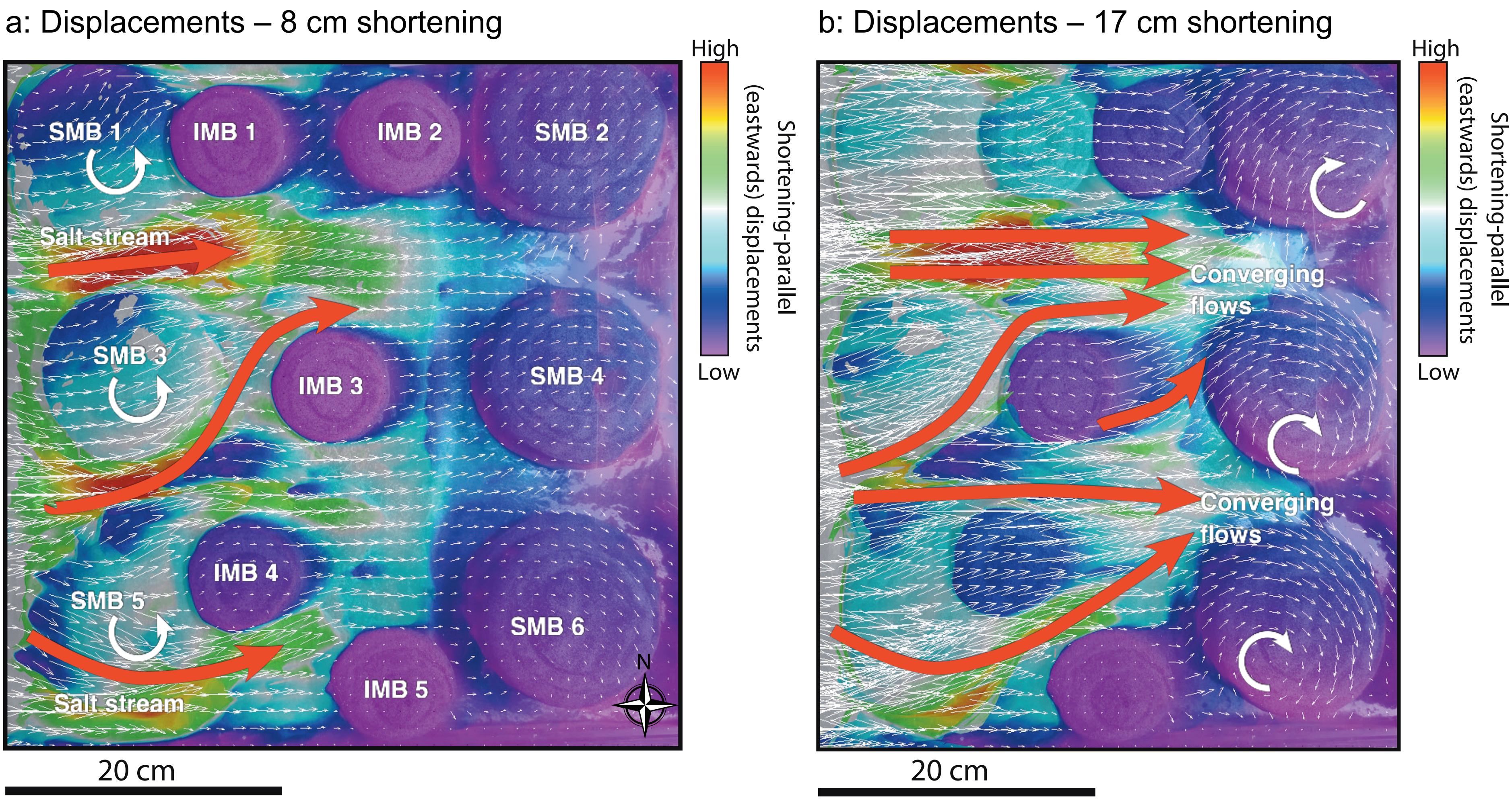

a: Displacements – 8 cm shortening
b: Displacements – 17 cm shortening
SMB 1
IMB 1
IMB 2
SMB 2
Salt stream
SMB 3
IMB 3
SMB 4
IMB 4
SMB 5
SMB 6
IMB 5
Salt stream
N
Converging
flows
Converging
flows
High
Low
Shortening-parallel
(eastwards) displacements
High
Low
Shortening-parallel
(eastwards) displacements
20 cm
20 cm

Figure 15

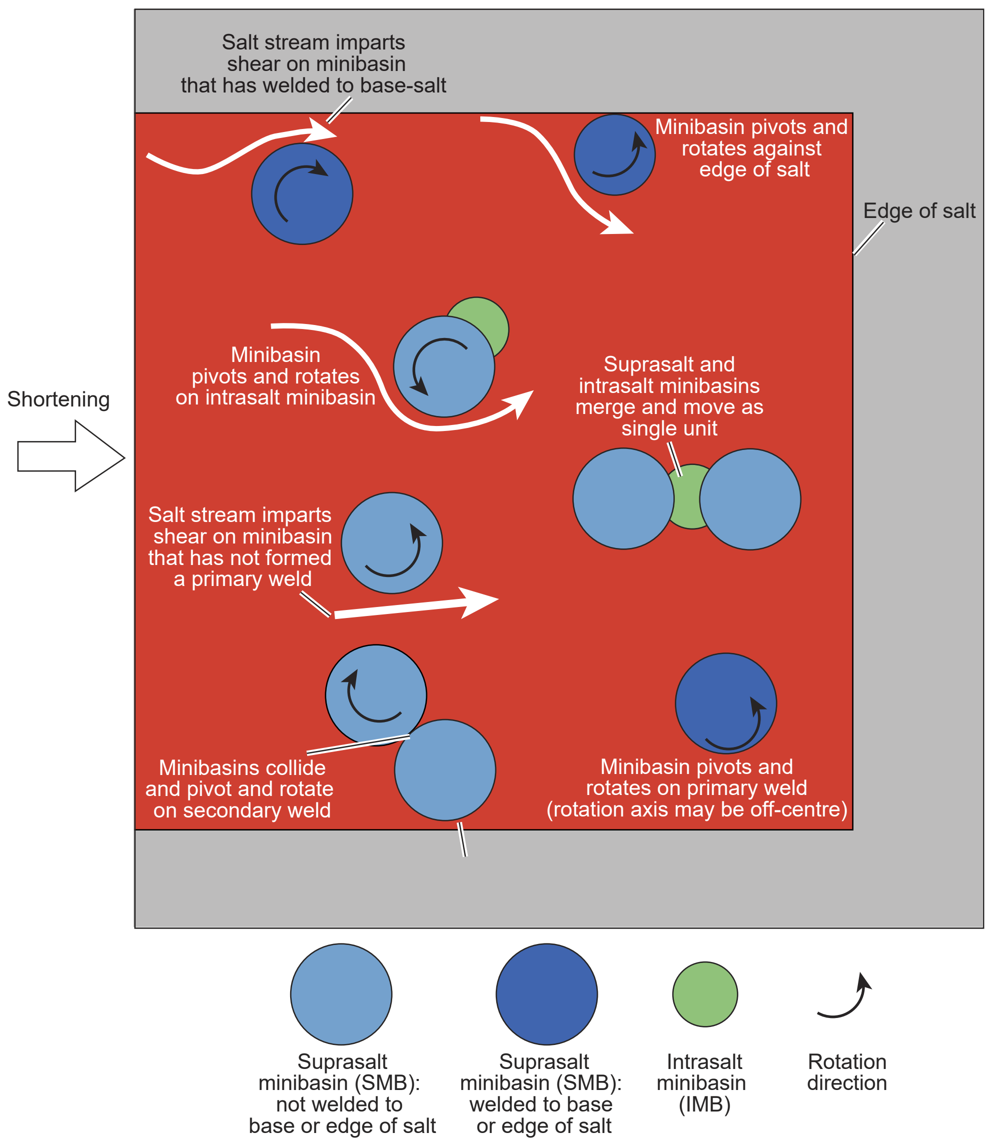

Salt stream imparts shear on minibasin that has welded to base-salt
Minibasin pivots and rotates against edge of salt
Edge of salt
Shortening
Minibasin pivots and rotates on intrasalt minibasin
Suprasalt and intrasalt minibasins merge and move as single unit
Salt stream imparts shear on minibasin that has not formed a primary weld
Minibasins collide and pivot and rotate on secondary weld
Minibasin pivots and rotates on primary weld (rotation axis may be off-centre)
Suprasalt minibasin (SMB): not welded to base or edge of salt
Suprasalt minibasin (SMB): welded to base or edge of salt
Intrasalt minibasin (IMB)
Rotation direction

Figure 16a

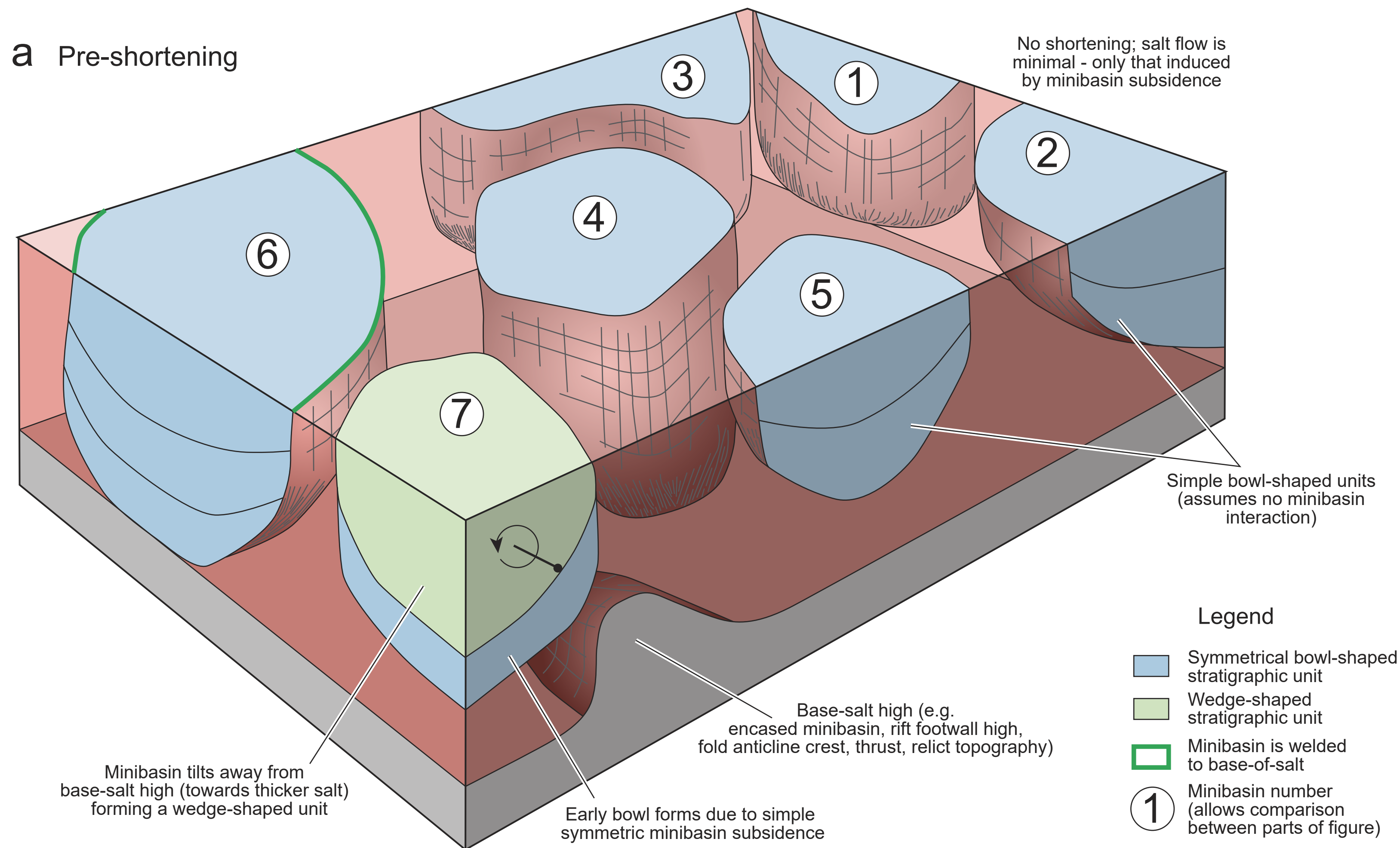
a Pre-shortening
No shortening; salt flow is
minimal - only that induced
by minibasin subsidence
1
2
3
4
5
6
7
Simple bowl-shaped units
(assumes no minibasin
interaction)
Base-salt high (e.g.
encased minibasin, rift footwall high,
fold anticline crest, thrust, relict topography)
Minibasin tilts away from
base-salt high (towards thicker salt)
forming a wedge-shaped unit
Early bowl forms due to simple
symmetric minibasin subsidence
Legend
Symmetrical bowl-shaped
stratigraphic unit
Wedge-shaped
stratigraphic unit
Minibasin is welded
to base-of-salt
1
Minibasin number
(allows comparison
between parts of figure)
Axis of tilt/rotation

Figure 16b

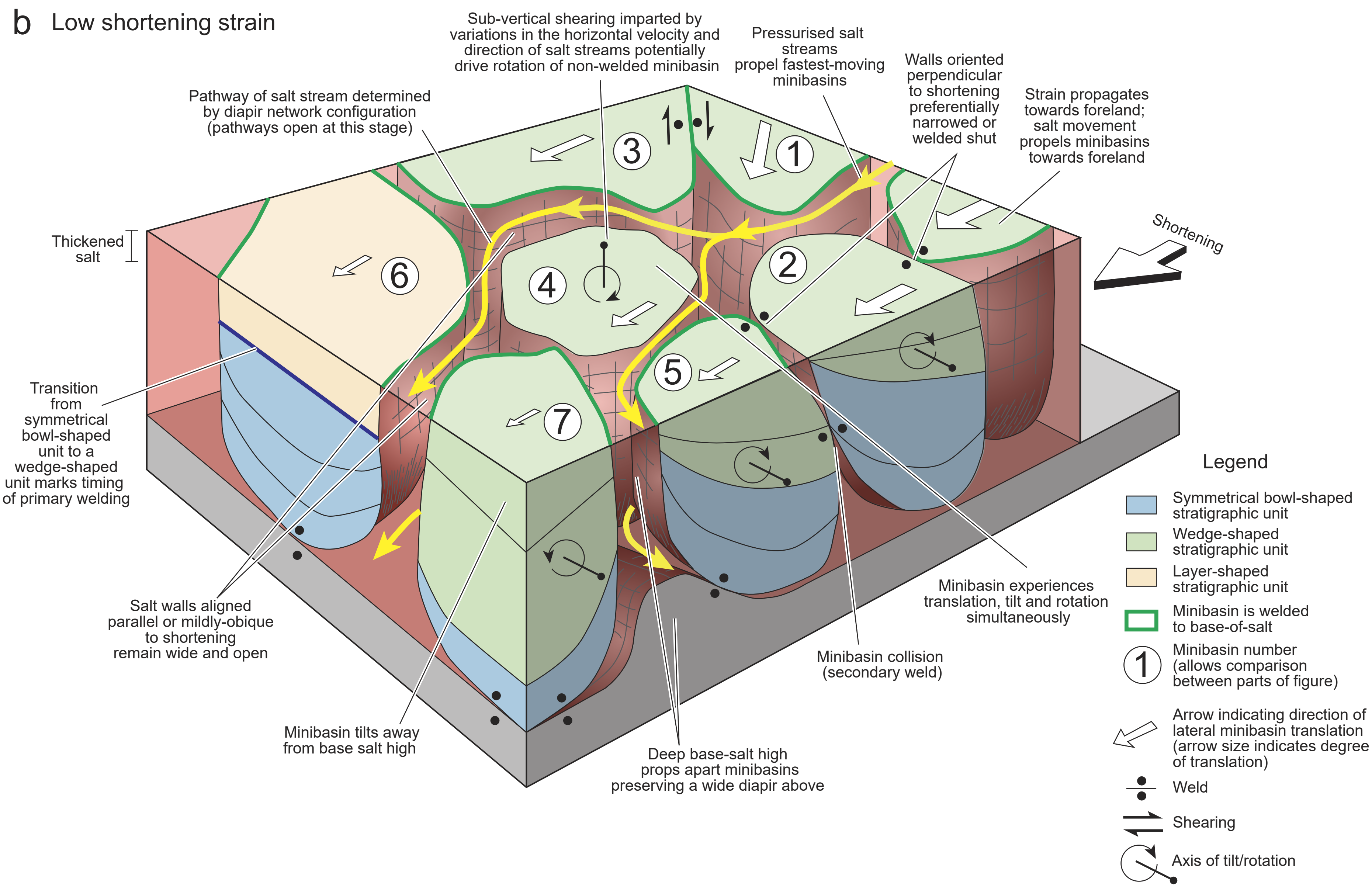

b Low shortening strain
Sub-vertical shearing imparted by variations in the horizontal velocity and direction of salt streams potentially drive rotation of non-welded minibasin
Pressurised salt streams propel fastest-moving minibasins
Walls oriented perpendicular to shortening preferentially narrowed or welded shut
Strain propagates towards foreland; salt movement propels minibasins towards foreland
Pathway of salt stream determined by diapir network configuration (pathways open at this stage)
Thickened salt
Shortening
1
2
3
4
5
6
7
Transition from symmetrical bowl-shaped unit to a wedge-shaped unit marks timing of primary welding
Salt walls aligned parallel or mildly-oblique to shortening remain wide and open
Minibasin tilts away from base salt high
Deep base-salt high props apart minibasins preserving a wide diapir above
Minibasin collision (secondary weld)
Minibasin experiences translation, tilt and rotation simultaneously
Legend
Symmetrical bowl-shaped stratigraphic unit
Wedge-shaped stratigraphic unit
Layer-shaped stratigraphic unit
Minibasin is welded to base-of-salt
Minibasin number (allows comparison between parts of figure)
Arrow indicating direction of lateral minibasin translation (arrow size indicates degree of translation)
Weld
Shearing
Axis of tilt/rotation

Figure 16c

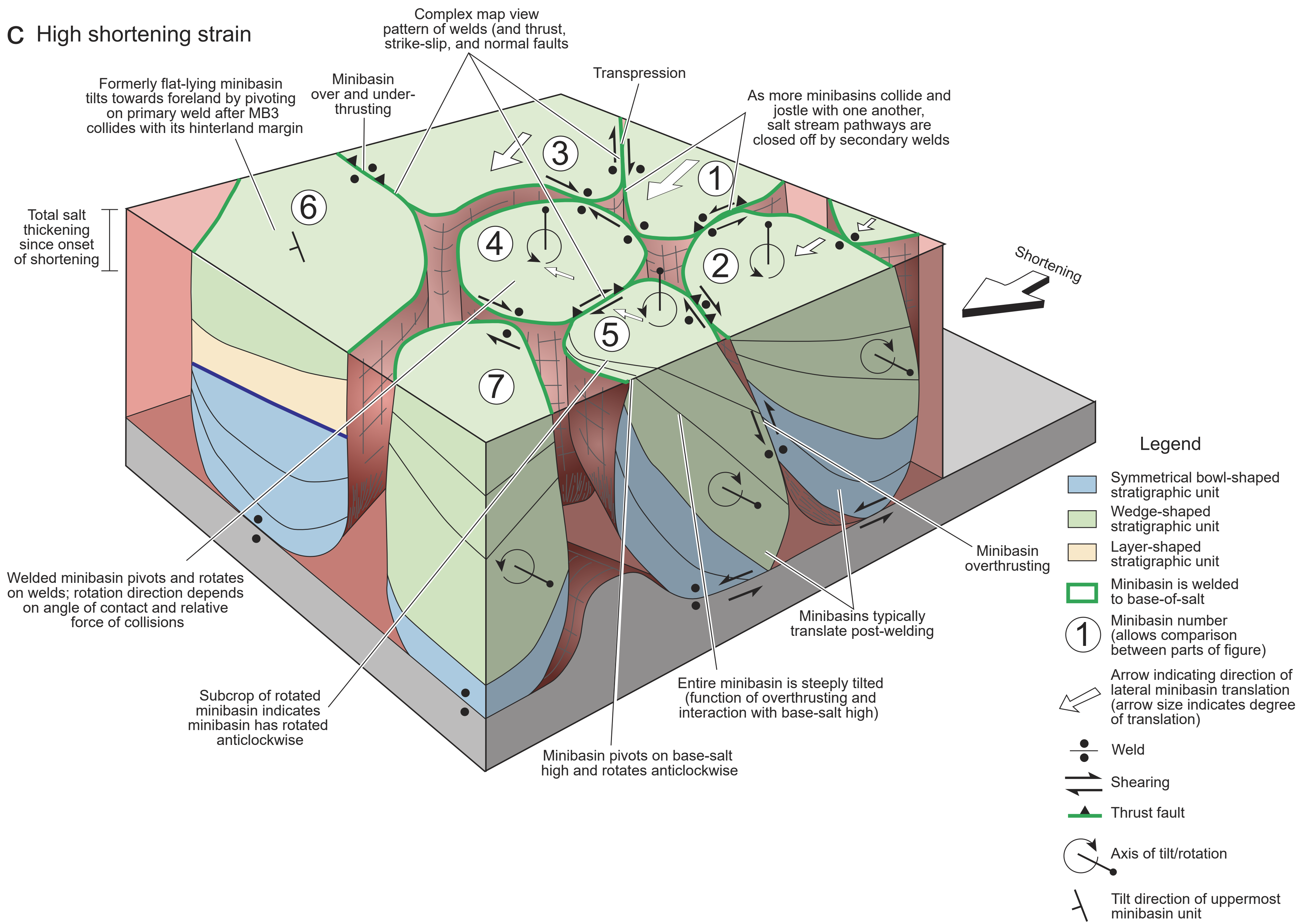
C High shortening strain
Complex map view pattern of welds (and thrust, strike-slip, and normal faults)
Transpression
Formerly flat-lying minibasin tilts towards foreland by pivoting on primary weld after MB3 collides with its hinterland margin
Minibasin over and under-thrusting
As more minibasins collide and jostle with one another, salt stream pathways are closed off by secondary welds
Total salt thickening since onset of shortening
Shortening
6
3
1
4
2
5
7
Welded minibasin pivots and rotates on welds; rotation direction depends on angle of contact and relative force of collisions
Subcrop of rotated minibasin indicates minibasin has rotated anticlockwise
Minibasin pivots on base-salt high and rotates anticlockwise
Entire minibasin is steeply tilted (function of overthrusting and interaction with base-salt high)
Minibasins typically translate post-welding
Minibasin overthrusting
Legend
Symmetrical bowl-shaped stratigraphic unit
Wedge-shaped stratigraphic unit
Layer-shaped stratigraphic unit
Minibasin is welded to base-of-salt
1
Minibasin number (allows comparison between parts of figure)
Arrow indicating direction of lateral minibasin translation (arrow size indicates degree of translation)
Weld
Shearing
Thrust fault
Axis of tilt/rotation
Tilt direction of uppermost minibasin unit

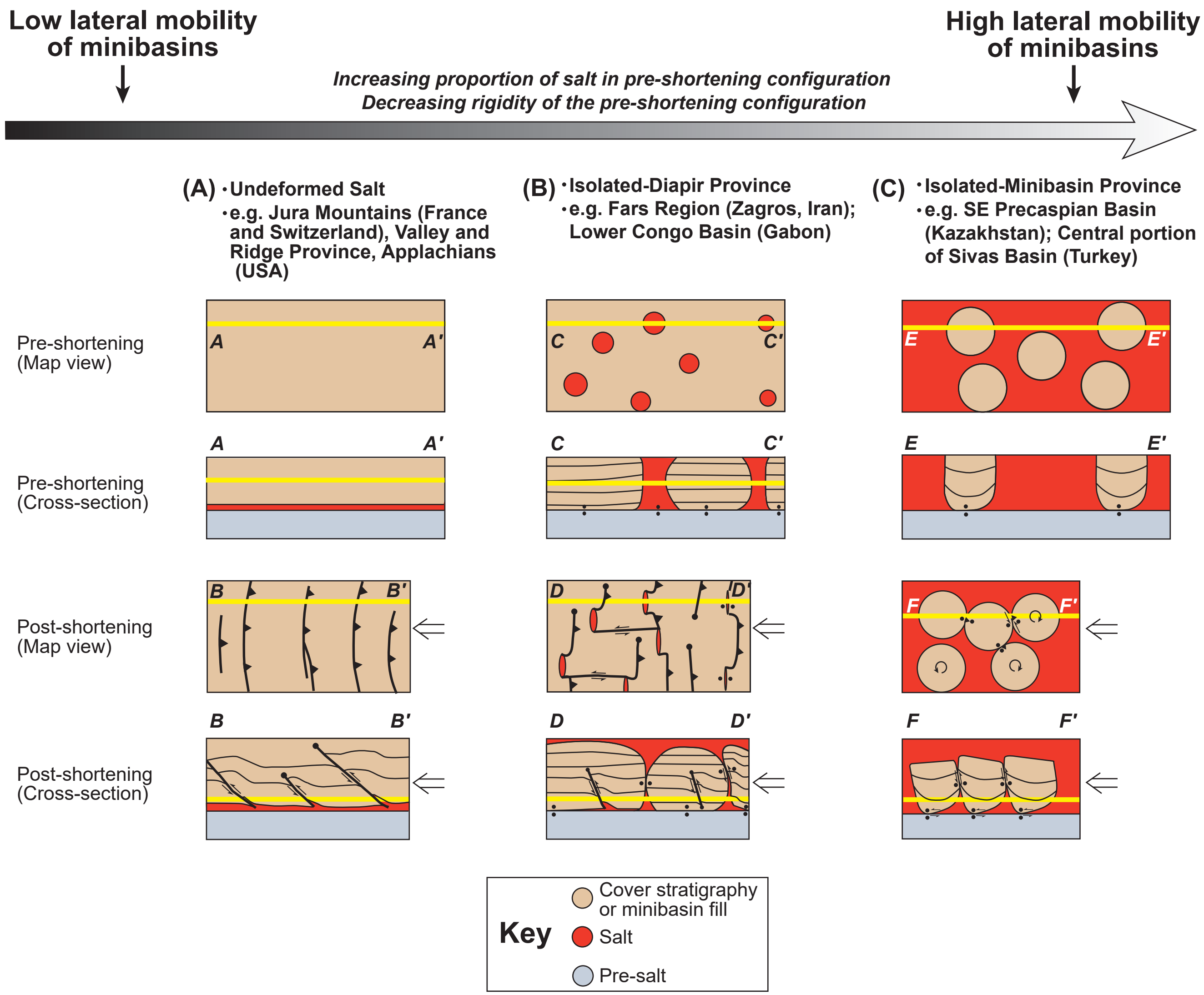

Low lateral mobility of minibasins
High lateral mobility of minibasins
Increasing proportion of salt in pre-shortening configuration
Decreasing rigidity of the pre-shortening configuration
(A) •Undeformed Salt
•e.g. Jura Mountains (France and Switzerland), Valley and Ridge Province, Applachians (USA)
(B) •Isolated-Diapir Province
•e.g. Fars Region (Zagros, Iran); Lower Congo Basin (Gabon)
(C) •Isolated-Minibasin Province
•e.g. SE Precaspian Basin (Kazakhstan); Central portion of Sivas Basin (Turkey)
Pre-shortening (Map view)
Pre-shortening (Cross-section)
Post-shortening (Map view)
Post-shortening (Cross-section)
A
A'
C
C'
E
E'
B
B'
D
D'
F
F'
Key
Cover stratigraphy or minibasin fill
Salt
Pre-salt